ASSESSMENT OF DEWATERING REQUIREMENTS FOR ÇALDAĞ
NICKEL MINE IN WESTERN TURKEY

A THESIS SUBMITTED TO
THE GRADUATE SCHOOL OF NATURAL AND APPLIED SCIENCES
OF
MIDDLE EAST TECHNICAL UNIVERSITY

BY

ÇİĞDEM CANKARA

IN PARTIAL FULFILLMENT OF THE REQUIREMENTS
FOR
THE DEGREE OF MASTER OF SCIENCE
IN
GEOLOGICAL ENGINEERING

OCTOBER 2011

Approval of the thesis:

ASSESSMENT OF DEWATERING REQUIREMENTS FOR ÇALDAĞ NICKEL MINE IN WESTERN TURKEY

submitted by **ÇİĞDEM CANKARA** in partial fulfillment of the requirements for the degree of **Master of Science in Geological Engineering Department**, **Middle East Technical University** by,

Prof. Dr. Canan Özgen _____
Dean, Graduate School of **Natural and Applied Sciences**

Prof. Dr. Erdin Bozkurt _____
Head of Department, **Geological Engineering**

Prof. Dr. Hasan Yazıcıgil _____
Supervisor, **Geological Engineering Dept., METU**

Examining Committee Members:

Prof. Dr. M. Zeki Çamur _____
Geological Engineering Dept., METU

Prof. Dr. Hasan Yazıcıgil _____
Geological Engineering Dept., METU

Assoc. Prof. Dr. M. Lütfi Süzen _____
Geological Engineering Dept., METU

Assist. Prof. Dr. Levent Tezcan _____
Geological Engineering Dept., HU

Dr. Koray K. Yılmaz _____
Geological Engineering Dept., METU

Date: **10.10.2011**

I hereby declare that all information in this document has been obtained and presented in accordance with academic rules and ethical conduct. I also declare that, as required by these rules and conduct, I have fully cited and referenced all material and results that are not original to this work.

Name, Last name: Çiğdem Cankara

Signature   :

ABSTRACT

ASSESSMENT OF DEWATERING REQUIREMENTS FOR ÇALDAĞ

NICKEL MINE IN WESTERN TURKEY

Cankara, Çiğdem

M.Sc., Department of Geological Engineering

Supervisor: Prof. Dr. Hasan Yazıcıgil

October 2011, 98 pages

The purpose of this study is to assess the dewatering requirements of planned open pit nickel mining at Çaldağ Site in Western Turkey. Dewatering is required for safe and efficient working conditions and pit wall stability. With this scope, a groundwater model of the study area is developed and used to predict the dewatering rate. The methodology mainly involves data collection, site hydrogeologic characterization and development of conceptual model, followed by construction and use of a groundwater model to predict the dewatering requirements of the mine site. The groundwater flow modeling is carried out using MODFLOW software and the dewatering simulations are carried out using MODFLOW Drain package. The drain cell configuration is determined by pit boundaries and invert elevations of drains corresponded to the bench elevations that will be achieved with respect to the mining schedule. In the transient model runs, monthly time steps were used. Using the outflow from in-pit drain cells, the

monthly dewatering rates are calculated. In order to assess the impacts of the hydraulic conductivity of the laterite on the pit inflow rates, simulations were carried out for different values of hydraulic conductivity of laterites. The predicted flow rate using the calibrated model is 107.54 L/s. A tenfold reduction in the hydraulic conductivity of laterite resulted in three fourths of decrease in the flow rate (24.42 L/s). Consequently, a wide range of flow rates for different hydraulic conductivity values of laterite was calculated. In order to confirm the hydraulic conductivity of laterites in the area, and to obtain a realistic dewatering rate, further pumping tests are needed.

Keywords: Groundwater modeling, Çaldağ, dewatering, pit inflow, MODFLOW, drain

ÖZ

BATI TÜRKİYE'DE YER ALAN ÇALDAĞ NİKEL MADENİ SAHASI İÇİN SUSUZLAŞTIRMA GEREKSİNİMLERİNİN DEĞERLENDİRİLMESİ

Cankara, Çiğdem

Yüksek Lisans, Jeoloji Mühendisliği Bölümü

Tez Yöneticisi: Prof. Dr. Hasan Yazıcıgil

Bu çalışmanın amacı Batı Türkiye'de yer alan Çaldağ Maden Sahası'nda yapılması planlanan açık ocak nikel madenciliğinin susuzlaştırma gereksinimlerinin değerlendirilmesidir. Susuzlaştırma, güvenli ve etkin çalışma koşulları ve ocak şev duraylılığı için gereklidir. Bu amaçla, çalışma alanının bir yeraltısuyu modeli geliştirilmiş ve susuzlaştırma debisinin belirlenmesinde kullanılmıştır. Çalışmada kullanılan yöntem temel olarak veri toplama, alanın hidrojeolojik karakterizasyonu, kavramsal modelin oluşturulması ve bunları takiben yeraltısuyu akım modelinin kurulması ile bu modelin sahanın susuzlaştırma gereksiniminin tahmini için kullanımını içermektedir. Yeraltısuyu akım modellemesi MODFLOW yazılımı ile yapılmış, susuzlaştırma simülasyonlarında ise MODFLOW Dren Paketi kullanılmıştır. Dren hücrelerinin konfigürasyonunu ocak sınırları belirlemiş

ve ocakların maden planına göre kazılması aylık zaman aralıklarıyla temsil edilmiştir. Ocakların içine yerleştirilmiş dren hücreleri kullanılarak susuzlaştırma debisi hesaplanmıştır. Çalışmada, lateritin hidrolik iletkenliğindeki belirsizlik nedeniyle susuzlaştırma simülasyonları lateritin farklı iletkenlik değerleri için tekrarlanmıştır. Lateritin kalibre edilmiş modeldeki hidrolik iletkenliği kullanılarak hesaplanan debi 107.54 L/s'dir. Lateritin hidrolik iletkenliğinde on kat bir azalma, debide dörtte üçlük bir düşüşe yol açmıştır (24.42 L/s). Sonuç olarak, lateritin farklı hidrolik iletkenlik değerleri için geniş bir aralıkta debiler hesaplanmıştır. Alandaki lateritlerin hidrolik iletkenliklerini doğrulamak ve gerçekçi bir susuzlaştırma debisi elde edebilmek amacıyla yeni pompa testlerinin yapılması gerekmektedir.

Anahtar kelimeler: Yeraltısuyu modellemesi, Çaldağ, susuzlaştırma, MODFLOW, dren

To My Beloved Family

ACKNOWLEDGEMENTS

TABLE OF CONTENTS

LIST OF TABLES

LIST OF FIGURES

FIGURES

CHAPTER 1

INTRODUCTION

1.1 Research Objectives

The development of a mine often means penetration of water table, causing inflows of groundwater to the mine. Mine dewatering was crucial for the miners even in Neolithic times, and where no dewatering techniques were available, the mine had to be closed down (Shepherd, 1993). Dewatering is required for safe and efficient mining conditions and pit wall stability. At Çaldağ Site in the western Turkey; nickel mining is planned and this study aims to assess the dewatering requirements of the project. Main objectives of this thesis are hydrogeological conceptualization of the groundwater system implemented in a numerical model, calibration of the model with existing field data, and prediction of flow rate to be applied in dewatering, using dewatering simulations. Within this scope, the groundwater flow model of the study area was developed and calibrated; using MODFLOW. Afterwards, excavation of three open pits was simulated via MODFLOW Drain Package. With evaluation of the results, dewatering requirement of the site and the rate at which dewatering will be achieved were predicted.

1.2 Geographical Location and Extent of the Area

The study area is located about 15 km north of Turgutlu in the Manisa Province, Western Turkey (Figure 1**).** It encloses an area of 76.7 km^2 and lies between UTM 4266070 – 4276980 N and UTM 563000 – 570031 E coordinates. The area lies in the Gediz Graben.

Figure 1 Location of the study area on Google Earth image

1.3 Information about Proposed Mining

In Çaldağ, mineral exploration started in 1940s mainly for iron mining. The discovery of nickel in the area dates back to 1970s; however due to relatively small size of the deposit and low-grade of nickel ore, nickel mining was not

considered to be economic at that time. In the beginning of 2000s, a demonstration plant was constructed in Çaldağ and atmospheric heap leaching using sulphuric acid was tested. The results demonstrated nickel heap leaching in Çaldağ as a low cost alternative to conventional nickel processing (Oxley et al., 2007).

In heap leaching method, a large heap of crushed ore is built and the heap is fed with acid solution from the top. Leaching is possible with various acids; however sulfuric acid is preferred due to mainly economical reasons. As the acid moves through the heap, metal particles in the ore are dissolved and taken into solution. The pregnant solution is collected at the bottom and treated chemically for metal recovery (Büyükakıncı and Topkaya, 2009). In the proposed methodology in Çaldağ; the sulphuric acid dissolves the nickel and cobalt, and iron is continually removed from the solution with the help of limestone. The iron free solution is returned back to the heap to increase the levels of nickel (Göveli, 2006).

As mentioned by Dağdelen and Güngör (2010), the most up to date resource evaluation was done by Snowden in 2008. According to this evaluation, the total mineable nickel reserve in Çaldağ is approximately 33.2 million tons with an average grade of 1.14% Ni. Together with nickel, besides other metals 0.07 % cobalt and 21.64 % iron production is expected.

The ore deposit in the area is divided into three pits: Hematite Pit, Pig Valley Pit and South Pit. The 15 years of production starts in the Hematite Pit (operates in three stages), continues with Pig Valley Pit (operates in three stages) and South Pit (operates in four stages), respectively. Other than the

three open pits, a leach pad and a waste rock storage area is located in the study area (Figure 2).
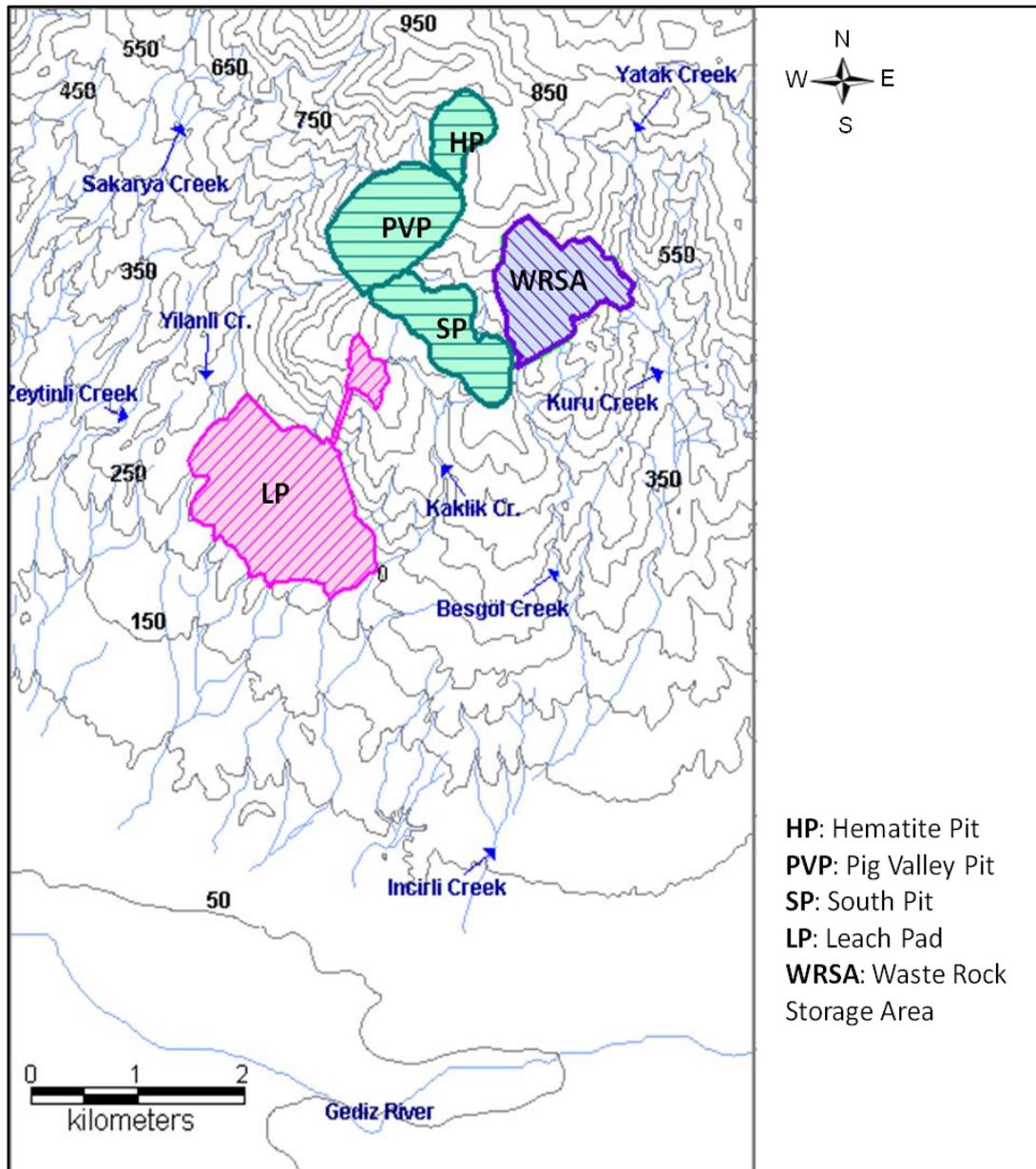
Figure 2 Locations of mine units on topographic map

The total surface area of the Hematite Pit is 315,400 m² and the total mineable reserve in this pit is 4.43 million tons. All three stages of this pit is planned to be completed in the first 3 years. The maximum water level in Hematite Pit is

about 867 m and the minimum pit bench elevation to be reached is 752 m, producing a maximum drawdown of 115 m for mining under dry conditions. In order to display the initial water levels together with topography and planned pit bottoms, cross sections were drawn; Figure 3 displays directions of these cross sections. It should be noted that the topography displayed in these cross sections is the initial topography before any excavation. In Figure 4; Cross Section 1-1', passing through all pits, is shown. After Hematite Pit is mined out in 3 years, it will be backfilled using some of the waste rock from Pig Valley Pit.
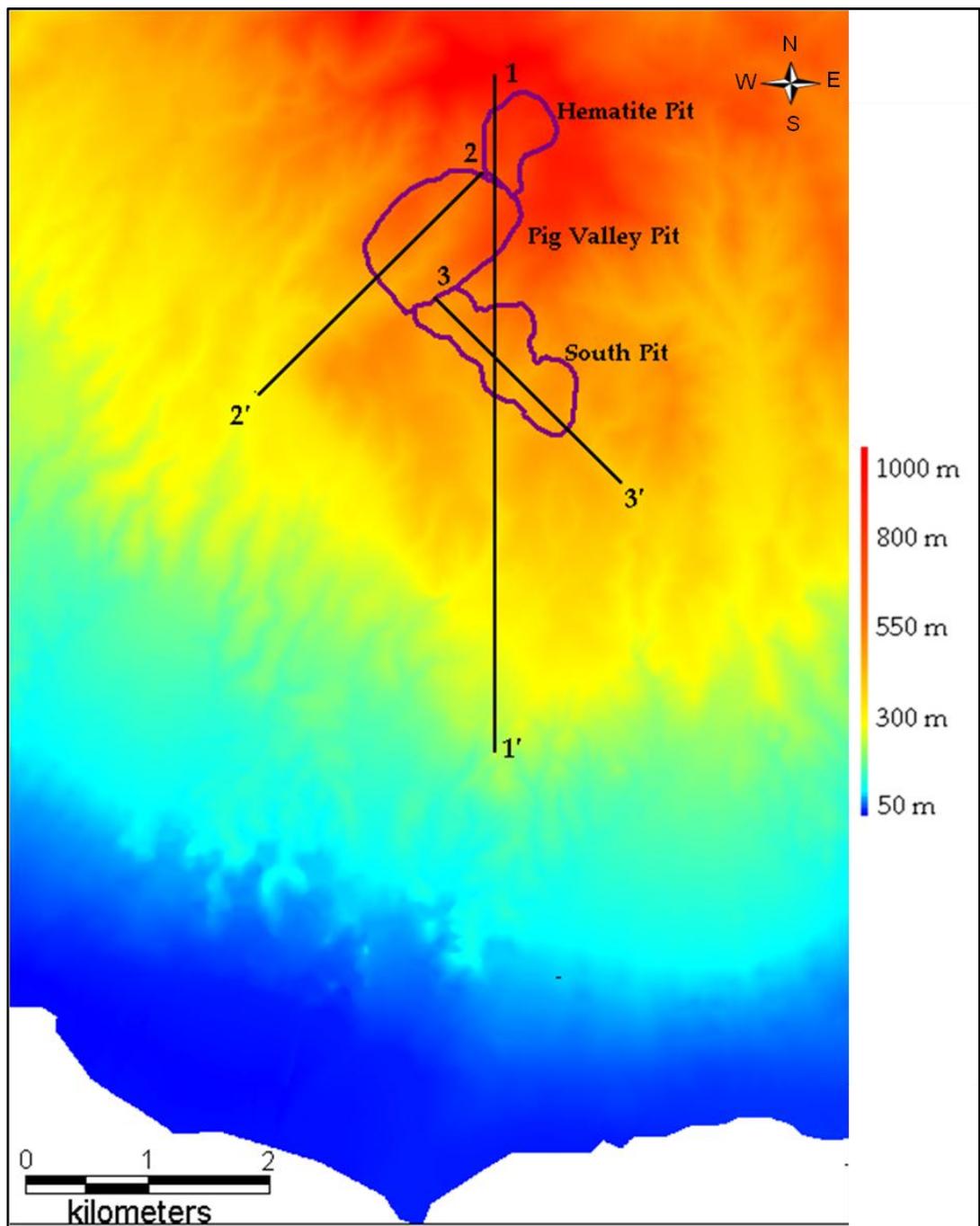
Figure 3 Directions of these cross sections
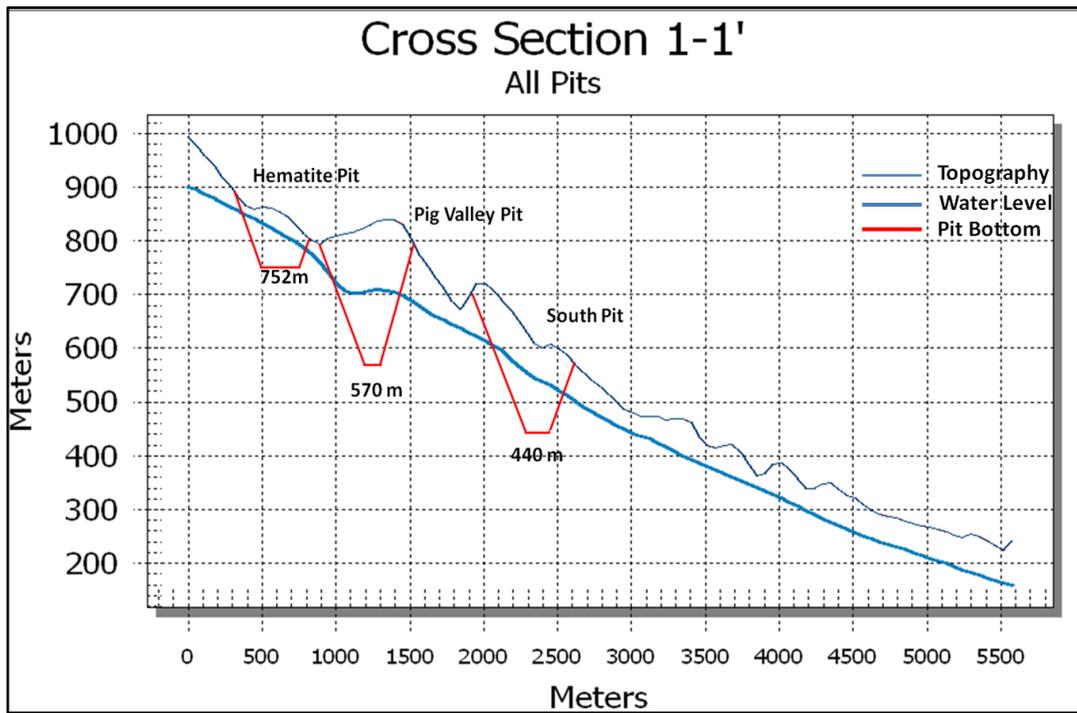
Figure 4 Cross Section 1-1' passing through all pits

Pig Valley Pit has a total surface area of 952,637 m² and the total mineable reserve in this pit is 19.07 million tons. First stage of this pit is planned to start operation in the 2nd year and the completion of all three stages is planned to be achieved in the 12th year. In the Pig Valley Pit, the maximum water level is around 783 m with minimum pit bench elevation of 500 m; in this pit maximum required drawdown is 283 m. In Figure 5, Cross Section 2-2' passing through Pig Valley Pit is shown. The completed stages of Pig Valley Pit will be backfilled with waste rock from its ongoing stages and from South Pit.
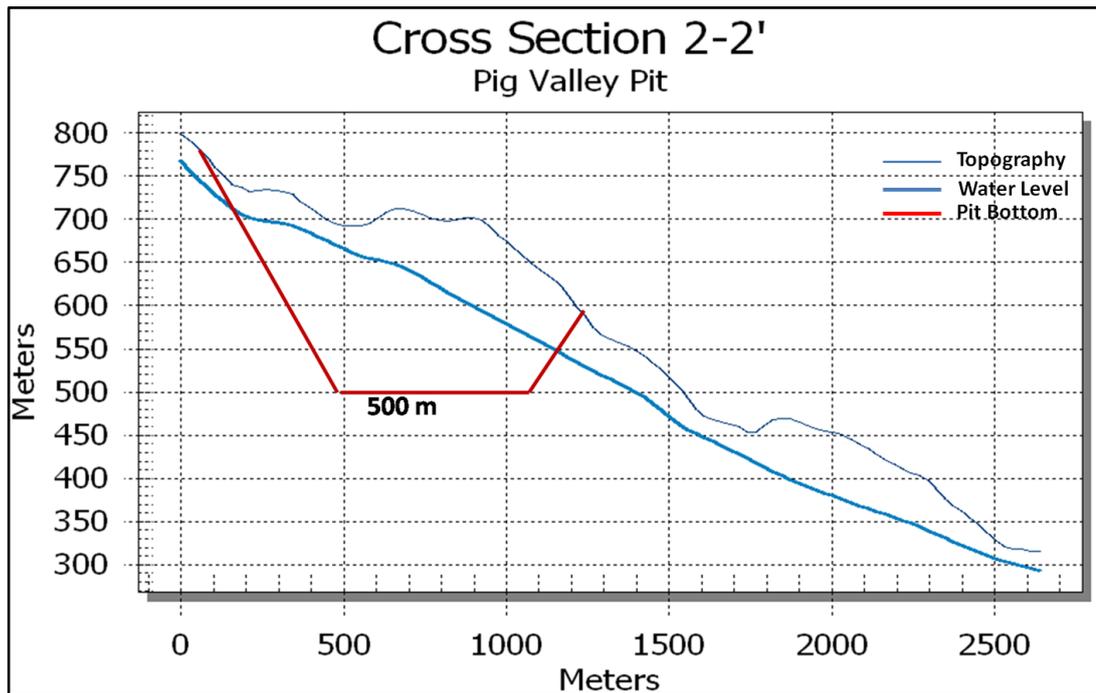
Figure 5 Cross Section 2-2' passing through Pig Valley Pit

The total surface area of the South Pit is 730,229 m² and the total mineable reserve is 9.72 million tons. Within the 6th year, initiation of production in the first stage of South Pit is planned and the completion is expected in the 15th year (end of mine life). The maximum water level in this pit is 649 m; minimum pit bench elevation producing the maximum required drawdown is 440 m. In Figure 6, Cross Section 3-3' which passes through South Pit is shown. During the progress of South Pit, completed stages will be backfilled with material from later stages being excavated.
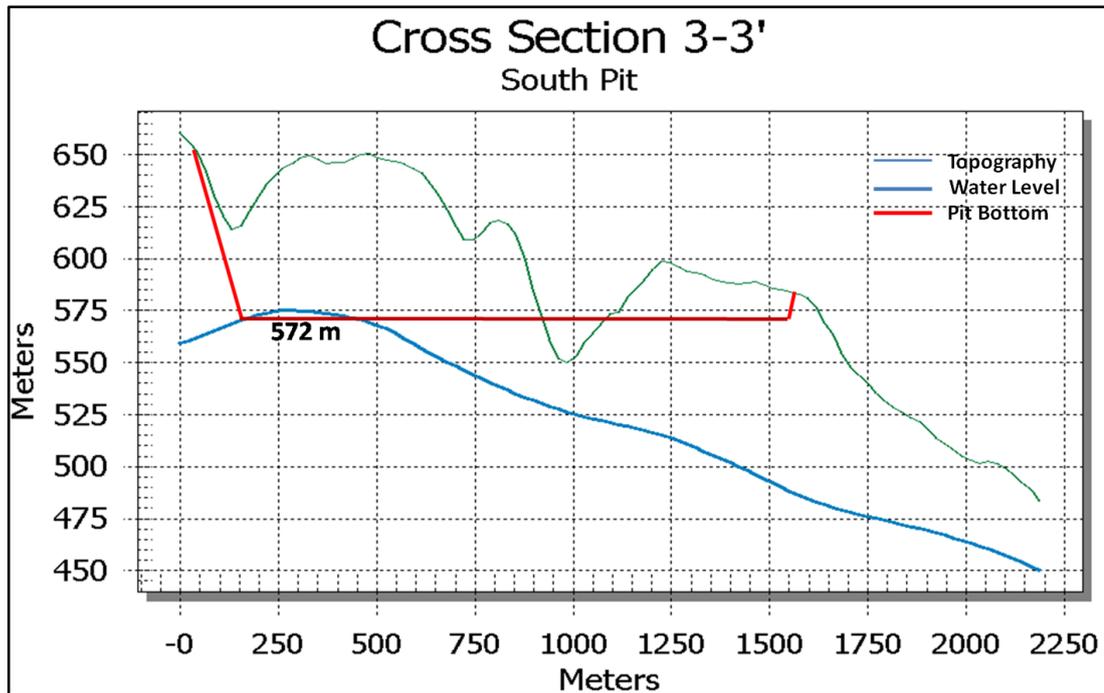
Figure 6 Cross Section 3-3' passing through South Pit

Surface area of the waste rock storage area is 1058.8 m². Here, the portion of waste rock which is not used in backfill of pits will be dumped. Finally, the surface area of the leach pad, where the crushed ore will be heaped and leached with acid, is 1533.2 m².

1.4 Previous Works

1.4.1 Previous Works Within and Around the Study Area

Since 20th century, various geological studies have been carried out within and around the Gediz Basin. Below, some of these studies are summarized.

11

The first geological study of the area dates back to 1915. In this study, Philippson determined the age of the micaschist, clayey greywacke, gabbro, diabase and limestone units as Paleozoic. In the following years, number of studies increased rapidly. 1/500,000, 1/100,000 and 1/25,000 scale geological maps of different parts of the region were prepared by the General Directorate of Mineral Research and Exploration (MTA). Related with the geology of the Gediz region, Bozkurt and Satır (2000); Yılmaz et al. (2000); Bozkurt and Sözbilir (2004); Bozkurt and Rojay (2005); Yanık et al. (2006); Çiftçi and Bozkurt (2009); and Thorne et al. (2009) carried out the most recent studies. Furthermore, there are many studies about the geothermal areas in the region.

District Office of State Hydraulic Works (DSİ) accomplished the earliest hydrogeological investigation in the area in 1983; namely The Hydrogeological Investigation Report for Gediz River Basin (Sarıgöl-Alaşehir, Salihli-Turgutlu and Akhisar-Manisa Plains). Rather than the whole surrounding region, more specific hydrogeological studies about Turgutlu region were performed by Bank of Provinces (İller Bankası) but they focus on the localities around the municipalities. In 2006, Turkish Environmental Consulting Company, ENCON conducted environmental baseline studies and completed the Environmental Impact Assessment (EIA) process in Çaldağ Mine Site. The most recent hydrogeological study in Çaldağ area was carried out by Yazıcıgil in 2008. In this area, any study regarding dewatering requirement of the mine was not carried out.

1.4.2 Previous Works about Dewatering Simulations

Mine dewatering was crucial for the miners even in Neolithic times, where no dewatering techniques were available, the mine had to be closed down (Shepherd, 1993). The search for gold, silver, copper, iron and precious stones sent people burrowing into the earth and thus into direct conflict with groundwater. With the dawn of the Industrial Revolution by the 18th century, the demand for coal was justifying all efforts to reach it. The British coal mines pushed deeper more difficult water conditions. Endless rope conveyors powered by horses on treadmills removed water in buckets. Starting with 1770s, first early steam engines were used in mine dewatering. It would be decades before wells with submersible electric pumps would be used. The submersible electric motor developed for military use in Russia in 1915 was used in dewatering of Berlin subway in the 1920s. Today, with appropriate regard to both theory and practice, effective dewatering can be accomplished under almost any field conditions (Wolkersdorfer, 2008).

Mine development often causes penetration of water table and results in groundwater flow into the mine. Dry working environments are preferred, as they maintain efficient mining conditions; improve slope stability and therefore safety (Van Mekerk, 1993).

The groundwater inflow to a mining excavation can be estimated using one of these techniques: equivalent well approach, two-dimensional flow equations or numerical techniques (Finite Difference Method, Finite Element Method, and Boundary Element Method). Equivalent well approach assumes that dewatering is achieved by use of an imaginary pumping well which fully penetrates the entire saturated thickness of the aquifer. From this

borehole, water is pumped out at a uniform discharge rate in order to lower the water level below the mining horizon at the mine boundary. Normally, the mine excavation is seen as a large diameter deep well. When a surface mine excavates below water table, groundwater flow into the excavation is inevitable and this flow regime is essentially two dimensional. Remote from the excavation, flow is linear but near the excavation there is vertical component of flow and it is non-linear. Thus, the result of equivalent well approach is very approximate. The two dimensional approach provides a factor of safety by estimating inflows to be slightly higher than the equivalent well approach and is a simpler tool (Singh and Reed, 1988). On the other hand, the differential equations that describe the physical phenomena can be solved analytically for limited class of problems and for their simple geometries. As indicated on the University of Stuttgart, Institute of Applied and Experimental Mechanics' Web site (http://www.iam.uni-stuttgart.de/bem/home_bem_introduc.html), more complex tasks require numerical approaches. They provide powerful predictive tools able to model a number of scenarios effectively. The application of finite difference, finite element and boundary element techniques in dewatering problems predict the quantities of inflow, clarify the pattern of water movement and identify regions where flow rates are particularly large (Singh and Reed, 1988).

In this study, the flow rate to be used in dewatering was determined by numerical modeling via modular finite difference groundwater flow model, MODFLOW (Harbaugh et al., 2000). The following paragraphs of this chapter assemble some of the studies in literature about determination of dewatering rates in mining, via different modeling software.

Hydrogeological assessment of the planned underground gold mining in Maud Creek Area, Northern Australia was carried out by Farrington and MacHunter (2007) . In the area, a previously mined open cut with a length of 200 m, width of 100 m and depth of 26 m, is located and it is estimated to contain 3×10^6 litres of water. After ten years of mining, the underground mine is expected to be 700 m deep. Since groundwater levels in the area are one to six meters below ground surface depending on topography, the pit will be dewatered prior to mining and during development. For calculation of groundwater inflows to the pit, groundwater modeling via MODFLOW with SURFACT was accomplished. Reflecting the monthly mine schedule, drain cells were used to obtain the amount of water to be abstracted and their distribution coincides with the extent of mineralization. The dewatering rate for the first year of mining was calculated to be 39.4 L/s and this rate progressively decreased to 19.7 L/s after ten years of mining.

In the feasibility study conducted for Galore Creek copper-gold-silver project in British Columbia, a numerical model was set up for open pit dewatering simulation (Bruce, 2006). In this study; with the aim of evaluating pit inflow rates and potential dewatering options, MODFLOW with SURFACT add-on was used. According to the author, SURFACT adds the capability of simulating variably-saturated flow to MODFLOW. In a model area of 300 km^2 four open pits are located and the mine life is projected to be 20 years. For the area to be dewatered; combination of vertical diameter wells, vertical in-pit wells and horizontal drains is planned. Operational open pit mining was input into the model by drains, which were activated to represent each year of mining. According to the model, the groundwater inflow rate, when there is no active dewatering, is approximately 27,000 m^3/day (312.5 L/s).

Furthermore, a second numerical model was constructed via FEFLOW in order to investigate the spacing of required horizontal drains (Bruce, 2006).

For the Diavik Diamond Mines located in the Canadian Shield, a numerical groundwater flow model was constructed by Kuchling et al. (2000) to predict groundwater inflow volumes and water quality with time. With this aim, MODFLOW and MT3DMS were used. Initial mine plan constitutes three open pit mines and underground mining which will continue afterwards, underneath two of the open pits. The timely changes in pit extents were integrated into the model by automatically adjusting the model boundaries every two years throughout the twenty year mine life. In this study, results of modeling indicated that the total mine inflows are expected to reach a maximum value of 9600 m^3/day (111.1 L/s) and TDS concentrations gradually increase in time to a maximum about 440 mg/L.

In 2001, Williamson and Vogwill constructed a three-dimensional groundwater model to predict the dewatering requirements associated with open-pit mining in the Lihir Gold Mine, New Guinea. The ore bodies in the area are located in a collapsed volcanic crater in an active geothermal field adjacent to sea, and for safe and efficient mining conditions together with pit wall stability, dewatering was required. It is important to note that when this study was carried out there was ongoing mining and dewatering operations in the field; this study had the aim of solving previously faced problems in dewatering. The constructed model included density and viscosity coupling to allow geothermal heat effects on groundwater flow to be simulated, and it was run in conjunction with a geothermal model. For a total drawdown of 200 m, the total required pumping rate was calculated to be 1000 L/s. In this

study, the final dewatering schedule in the mine area constitutes 8 dewatering bores with average depth of 275 m (pumping rate of each ranging from 50 to 130 L/s) and over 100 horizontal drainholes up to 200 m long (with rates up to 5 L/s).

CHAPTER 2

DESCRIPTION OF THE STUDY AREA

2.1 Morphology

The study area is located within the Aegean Region. It is characterized by steep and undulating topography, with an altitude ranging from 50 m above sea level in the south, to 1034 m at Ayşekızı Hill in the north. Hills with significant elevations in the study area include Akyatak Hill (960 m), Sırayatak Hill (790 m), Sakar Hill (625 m) and Taşgöl Hill (590 m). Considering the hills in the area as check points, Digital Elevation Model (DEM) enclosing the study area was modified from Ağartan (2010). It was created from a 1/25,000 scaled topographic map with 12.5 m grid size using MapInfo 8.5 Software (Figure 7).
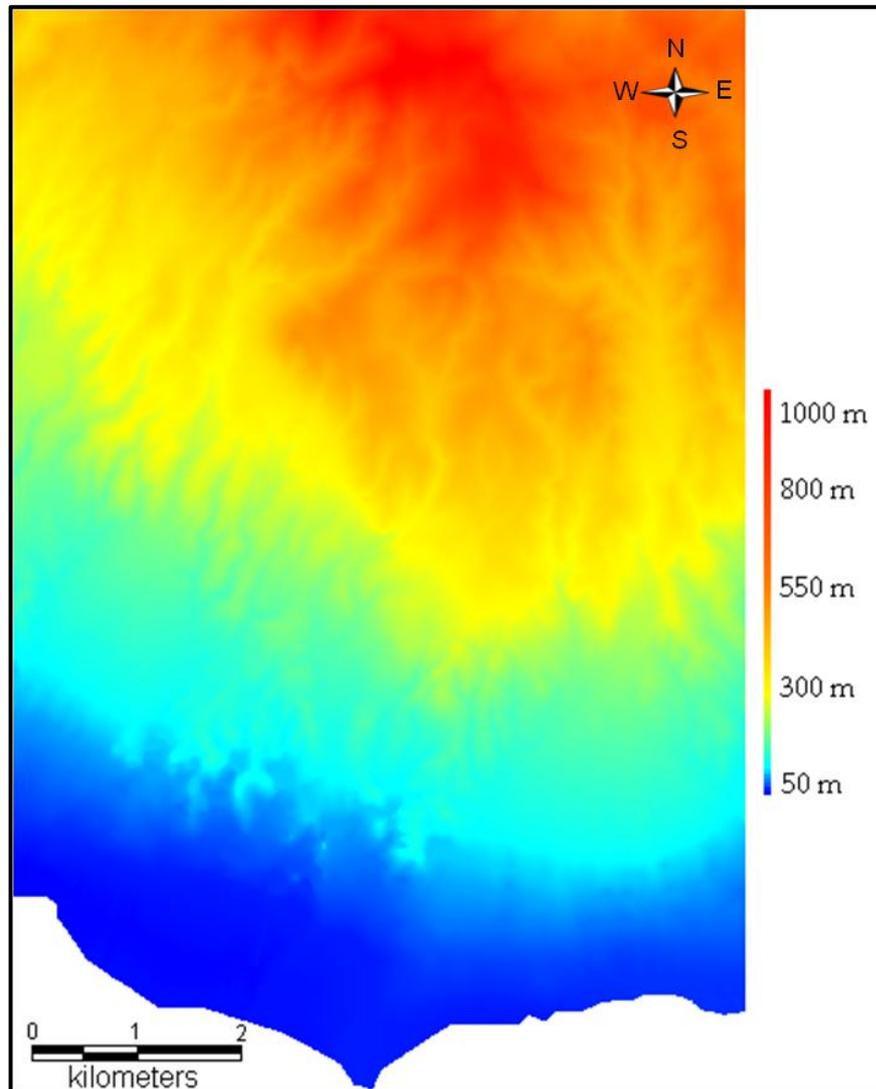
Figure 7 Digital Elevation Model (DEM) of the model area

2.2 Climate and Meteorology

Conformable with the climatic conditions of Aegean Region in which the area is located; the climate is mild with soft springs, hot and dry summers, sunny autumns and warm winters with occasional showers. Due to the character of Aegean Region with mountains perpendicular to the shores, sea

climate (similar to Mediterranean climate) reaches inner parts of the region where continental climate is more dominant. Thus, the study area is characterized by a typical Mediterranean climate with relatively high average annual temperatures. Due to high altitudes in northern parts, temperatures slightly cooler than the rest of the region are experienced with some snow and frost days.

Around the area; six meteorological stations, established by the State Meteorological Organization (DMI), are present at Manisa, Akhisar, Salihli, Saruhanlı, Gölmarmara and Turgutlu (Figure 8). Manisa, Akhisar and Salihli stations are principal meteorological stations which measure hourly temperature, solar radiation, wind speed and direction, three times daily precipitation and monthly maximum precipitation. Saruhanlı, Gölmarmara and Turgutlu are ordinary meteorological stations which measure temperature, wind speed and direction, and precipitation (three times daily and daily total). Detailed information about meteorological stations is given in Table 1.
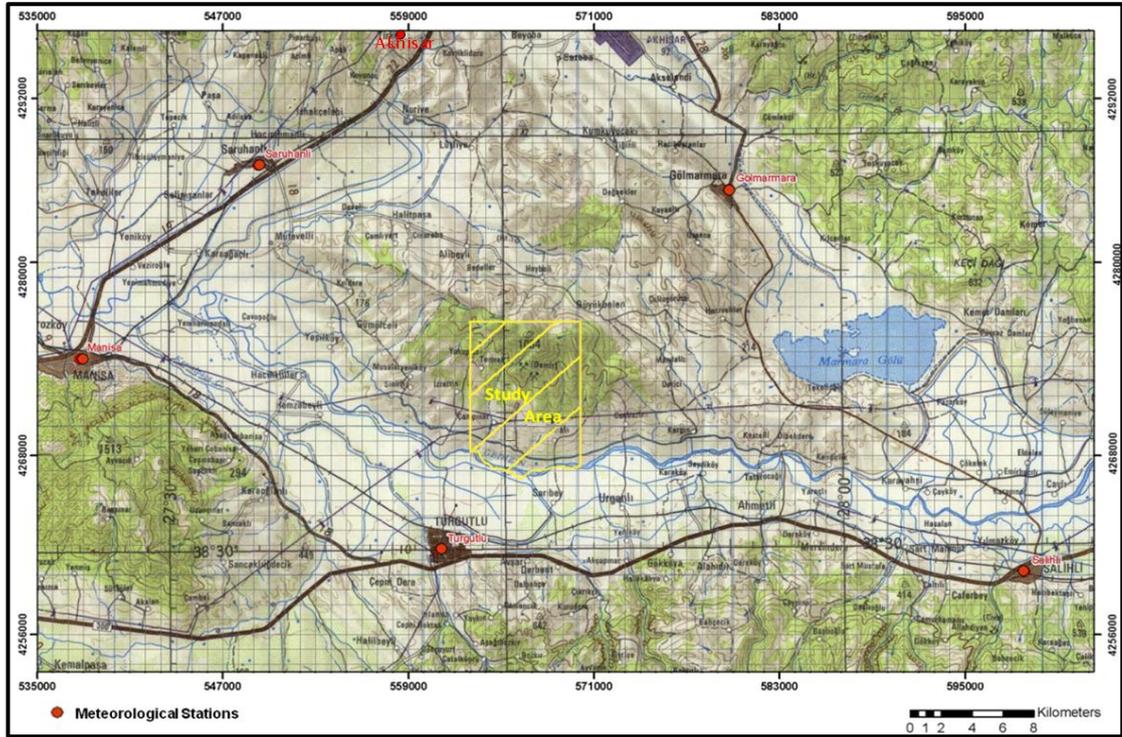
Figure 8 Meteorological stations around the study area (Modified from (Yazıcıgil, 2008).

Table 1 Detailed information about meteorological stations

	Station Number	X-Coordinate	Y-Coordinate	Period of Data Availability	Elevation (m)
Saruhanlı	5269	549301	4287516	1986-1995	-
Gölmarmara	5273	579741	4285913	1984-1991	-
Turgutlu	5615	561087	4261704	1984-2006	120.000
Akhisar	17184	570865	4306176	1937-2006	92.034
Manisa	17186	537773	4274507	1930-2006	71.000
Salihli	17792	598897	4260231	1939-2006	111.000

2.2.1 Temperature

The average annual temperature in the region is 16.34°C. January and February are the coldest months with average monthly minimum temperature of -4.44 °C; while July is the hottest month with average monthly maximum temperature of 39.76 °C. In Table 2; average monthly minimum and maximum temperature values together with monthly minimum and maximum observed ones are given for the regional network.

Table 2 Monthly minimum and maximum observed, average monthly minimum and maximum temperature values for the regional network

	Saruhanlı	Gölmarmara	Turgutlu	Akhisar	Manisa	Salihli
Min. Monthly Temp. °C	-8.2	-7.8	-10	-13.2	-13.1	-13.5
Month & Year of Observation	Feb 1992	Feb 1985	Feb 2004	Jan 1954	Jan 1954	Feb 2004
Max. Monthly Temp. °C	42	43.2	44.9	44.6	45.1	44.8
Month & Year of Obs.	Jul 1987	Jul 1987	Jul 2000	Aug 1958	Jul 2000	Jul 2000
Ave. Min. Monthly Temp. °C	-5.13	-4.06	-3.81	-5.25	-4	-4.4
Month of Obs.	Feb	Feb	Jan	Jan	Jan	Jan
Ave. Max. Monthly Temp. °C	39.76	39.6	39.93	39.83	40.02	39.42
Month of Obs.	Jul	Jul	Jul	Jul	Jul	Jul
Ave Temp. °C	15.9	16.3	16.7	16.1	16.9	16.3

2.2.2 Relative Humidity

The average relative humidity for all State Meteorological Organization (DMI) stations varies from about 46% in June and July, to 75 % in December, with a yearly average of 60% (Table 3). Among the stations in the region, Akhisar has the highest humidity whereas Gölmarmara has the lowest. The average monthly relative humidity for each station is displayed in Figure 9.

Table 3 Average monthly relative humidity for stations

	Saruhanlı	Gölmarmara	Turgutlu	Akhisar	Manisa	Salihli
Min. Monthly Relative Humidity (%)	36.8	34.1	33	37.8	35.5	39.8
Month & Year of Observation	Jul 1994	Jul 1985	Jun 2001	Jun 2003	Jul 1945	Jun 2001
Max. Monthly Relative Humidity (%)	83.2	76.2	82.5	86.3	88.2	86.3
Month & Year of Obs.	Dec 1990	Dec 1985	Dec 2004	Dec 1950	Dec 1950	Jan 1982
Average Min. Relative Humidity (%)	44	38.46	47.99	50.49	44.55	50.22
Month of Obs.	Jul	Jun	Jul	Jul	Jul	Jun
Ave. Max. Relative Humidity (%)	76.06	71.7	76.84	76.84	76.22	75.17
Month of Obs.	Dec	Dec	Dec	Dec	Dec	Dec
Ave.Relative Humidity (%)	58.5	53.4	61.5	63.9	60.9	62.7

	Jan	Feb	Mar	Apr	May	Jun	Jul	Aug	Sep	Oct	Nov	Dec
Saruhanlı	74.23	67.99	62.31	57.92	51.55	44.49	44	45.76	48.4	59.88	69.8	76.06
Gölmarmara	68.74	64.53	58.97	51.33	46.3	38.46	39.04	39.74	41.5	53.34	66.57	71.7
Turgutlu	73.42	70.45	65.32	62.27	56	48.4	47.99	49.63	53.58	62.56	71.13	76.84
Akhisar	75.65	72.08	67.73	64.2	59.81	52.09	50.49	52.2	56.48	65.53	73.91	76.84
Manisa	74.73	70.25	66	61.6	56.36	47.7	44.55	46.1	51.91	62.61	72.73	76.22
Salihli	73.94	69.82	66.61	61.67	56.47	50.22	51.23	53.64	56.96	65.72	71.19	75.17

Figure 9 Average monthly relative humidity graph for each station

2.2.3 Precipitation

The distribution of average monthly precipitation for the stations in the regional network is shown in Figure 10. December is the wettest month for each station, and except Gölmarmara station, August is the driest month. The dry summer period extends from June through to early September, and the wet winter period extends from November to February.

26
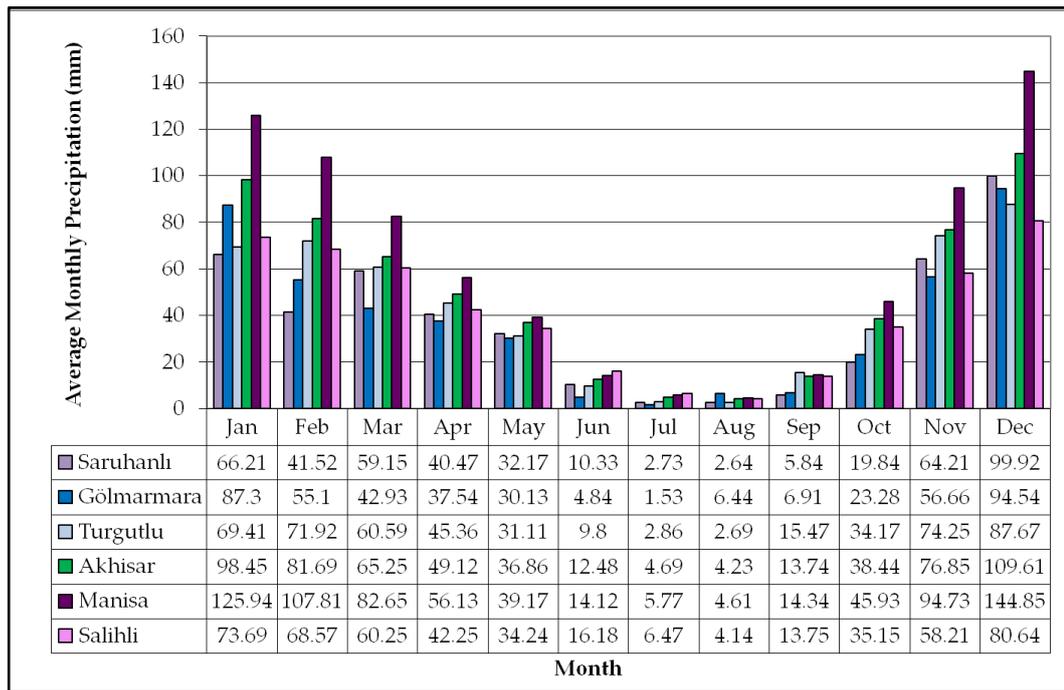
Figure 10 Distribution of average monthly precipitation for the stations in the regional network

On an annual basis, data show that Manisa is the station that receives most precipitation (736 mm/year), while Saruhanlı (445 mm/year) and Gölmarmara (447 mm/year) receive the least. This is probably due to the availability of a longer period of record (1943-2006) at Manisa station which includes a series of wet and dry years, giving a representative average annual value. The same is also true for Salihli (1939-2006) and Akhisar stations (1943-2006) where long term data is available. The short term data collected at Saruhanlı (1986-1995) and Gölmarmara (1984-1991) correspond to a long-term dry period that was present in the region from 1982 to 1996.

27

2.2.4 Evaporation

In the region, evaporation is only monitored at Akhisar and Salihli stations. The monitoring is usually carried out from April to November. Hence there were missing data belonging to the months with low evaporation. These missing data were calculated by correlation between measured monthly evaporation and average monthly temperature data, where available. The average monthly evaporation values at Salihli and Akhisar stations are plotted in Figure 11. In July and January, the average monthly maximum and minimum evaporations were observed, respectively. In addition, the yearly average evaporation was calculated as 1377 mm (Yazıcıgil, 2008).

	Jan	Feb	Mar	Apr	May	Jun	Jul	Aug	Sep	Oct	Nov	Dec
Akhisar	26.29	31.94	50.89	94.17	150.8	213.3	265.8	249.9	176	97.81	42.93	29.14
Salihli	3.28	3.69	29.16	102.2	165.8	221.2	258.3	238.3	164.1	95.09	34.93	8.42
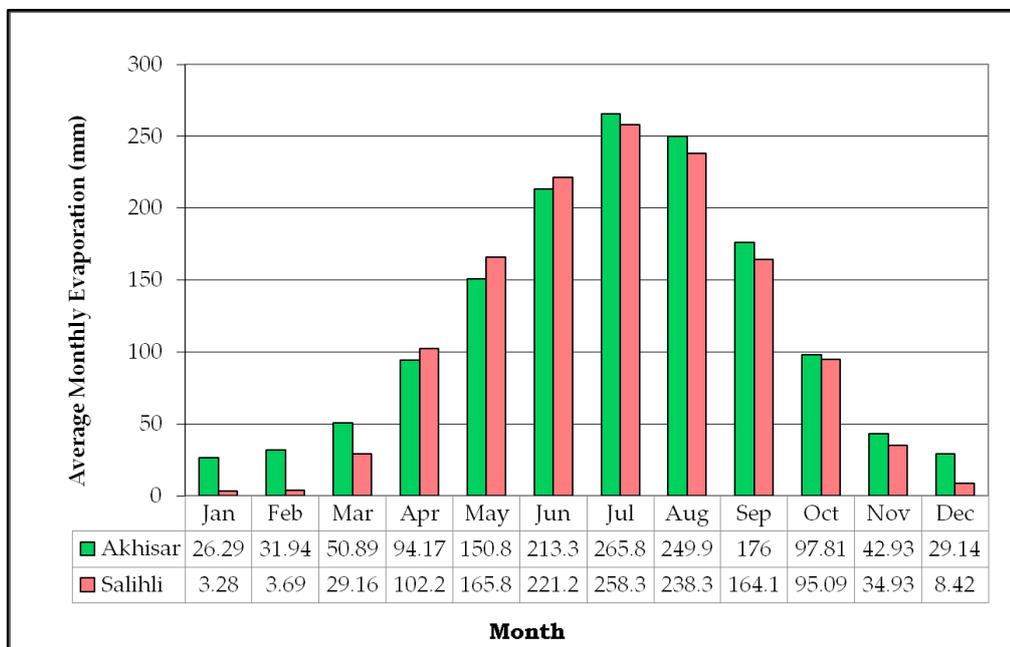
Figure 11 Average monthly evaporation at Salihli and Akhisar stations

2.2.5 Wind

Monthly wind speed data for Akhisar, Manisa and Salihli stations indicate that the average annual wind speeds range between 1.0 m/s and 3.0 m/s. In July and August, generally the highest wind speeds are observed (Figure 12).

	Jan	Feb	Mar	Apr	May	Jun	July	Aug	Sep	Oct	Nov	Dec
Akhisar	1.22	1.59	1.72	1.33	1.29	1.53	1.98	1.98	1.40	0.76	0.57	0.88
Manisa	1.95	2.19	2.13	1.94	1.82	1.93	2.17	2.10	1.80	1.58	1.45	1.72
Salihli	1.32	1.52	1.57	1.60	1.69	1.84	2.01	1.87	1.52	1.19	1.12	1.22
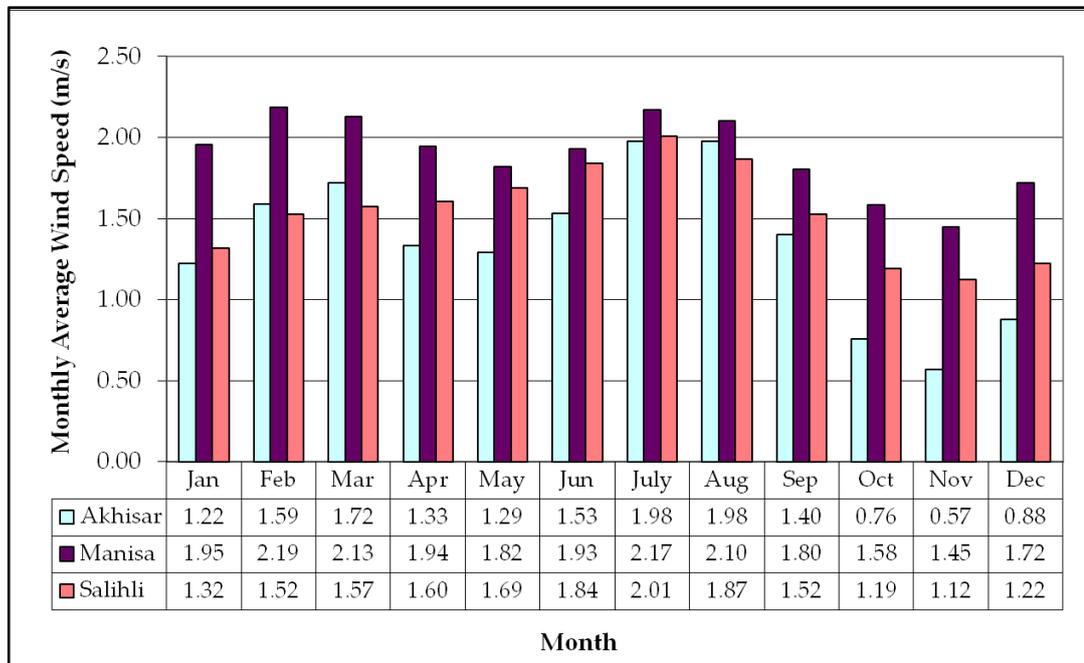
Figure 12 Average monthly wind speed

2.3 Geology

2.3.1 Regional Geology

Western Turkey is known to be the site of widespread active N-S continental extension. Forming the eastern part of Aegean extensional province, the region is currently under the influence of forces resulting from convergence of African and Eurasian plates. The region has been subjected to this N-S extension since, at least, latest Oligocene-Early Miocene. The outstanding structures of the area are; E-W trending grabens and intervening horsts, exposing the Menderes Massif (Bozkurt and Sözbilir, 2004). The Menderes Massif is one of the two large metamorphic culminations within the Alpine Orogen of Turkey, the other one being the Kırşehir Massif (Bozkurt and Satir, 2000). It is geographically divided into three sub-massifs along E-W trending Gediz and Büyük Menderes Grabens (Figure 13), as northern, central and southern (Bozkurt and Rojay, 2005).
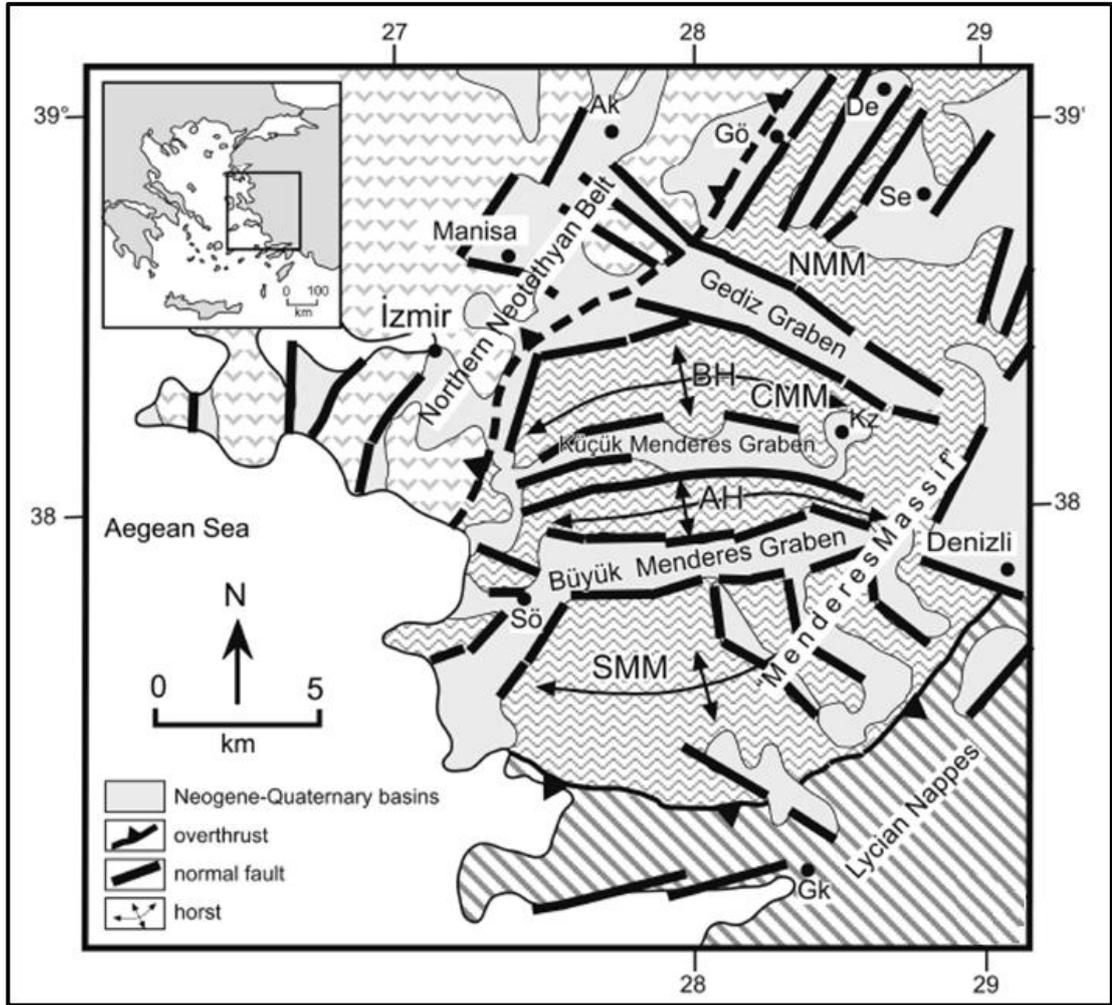
Figure 13 Outline geological map of western Anatolia showing Neogene and Quaternary basins and subdivision of the Menderes Massif. The sequences of Miocene and Pliocene age are not differentiated. BH- Bozdağ horst, AH- Aydın Horst, CMM- Central Menderes Massif, NMM- Northern Menderes Massif, SMM- Southern Menderes Massif, Ak- Akhisar, Gö- Gördes, De- Demirci, Se- Selendi, Kz- Kiraz, Gk- Gökova, Sö- Söke. (Modified from Bozkurt and Rojay, 2005)

The area focused in this study (Çaldağ Region) is located on the northern edge of Menderes Massif, on a horst block to the north of Gediz Graben (Thorne, et al., 2009). Gediz Graben starts southeast of Alaşehir to the east

and extends westward for more than 100 km to Turgutlu and beyond, along the plain of Gediz River. It is probably the best developed graben in Turkey, regarding the accumulated sediment thickness and total offset along the graben-boundary structures (Çiftçi and Bozkurt, 2009). The E-W trending graben is asymmetric with steeper and seismically more active southern margin (Yilmaz et al., 2000).

The rock units exposing in the vicinity of Gediz Graben can simply be grouped into two, as basement and cover units. Metamorphic rocks of the Menderes Massif constitute the pre-Neogene basement. Above them; cover units of ages varying from Miocene to Recent, lie unconformably (Çiftçi and Bozkurt, 2009).

2.3.2 Site Geology

Çaldağ occurs as an isolated mountain sequence consisting of various geological units surrounded by a plain of young sediments. From oldest to youngest, the rock units cropping out in the study area include: rocks belonging to the İzmir-Ankara Suture Zone (Brinkman, 1966), laterites formed over the ultrabasic rocks of this zone, Kanlıtepe Formation consisting of lacustrine and fluvial sediments (Yanık et al., 2006) and alluvium unconformably overlying all these units (Figure 14).
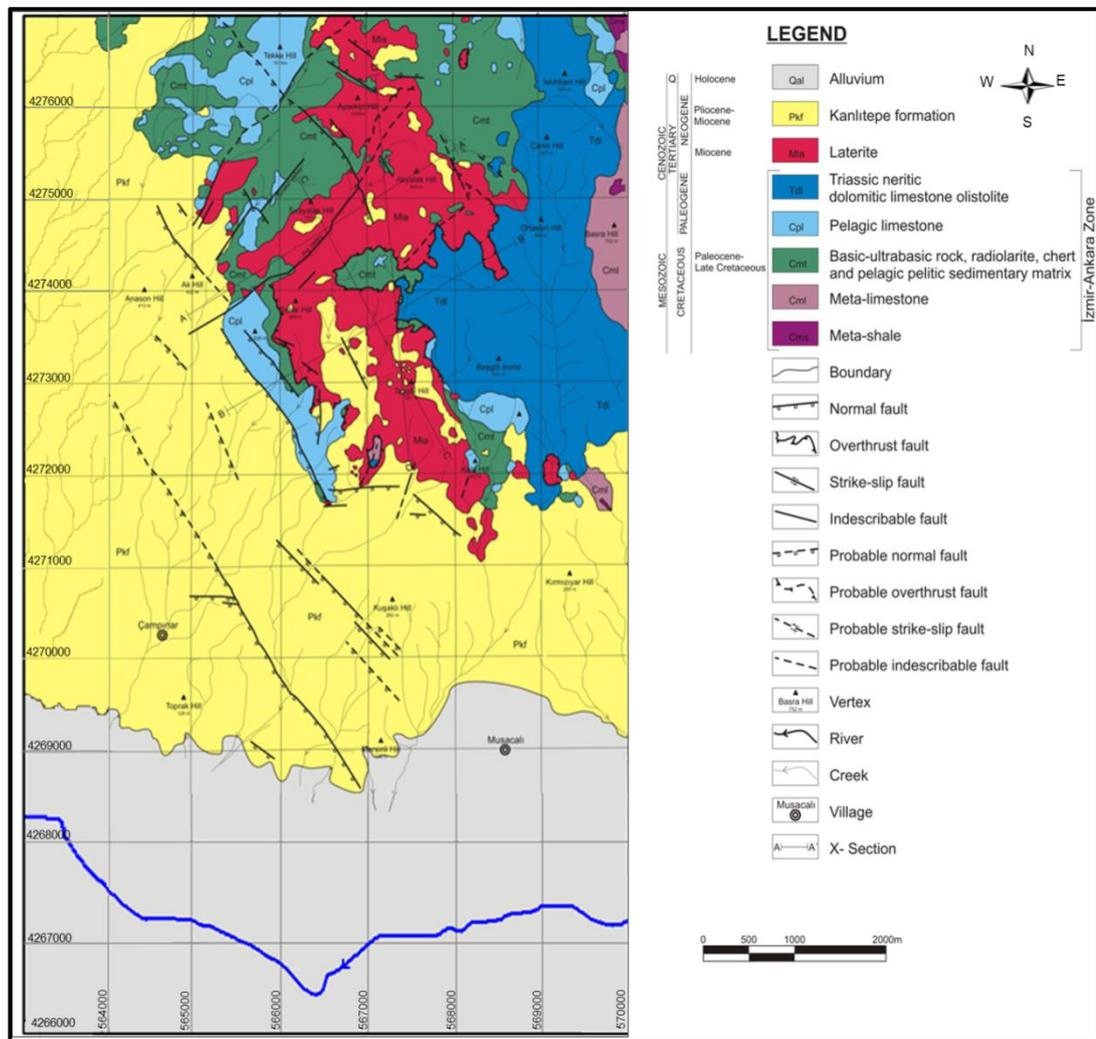
Figure 14 Geological map of the study area (Modified from (Yazıcıgil, 2008) using MTA map)

İzmir-Ankara Suture Zone rocks are Late Cretaceous-Paleocene aged, and are part of an accretional prism consisting of ultrabasic, serpentinized ultrabasic and spilitic volcanic rocks with pelagic matrix. The matrix consists of sandstone, mudstone, claystone, limestone, radiolarite and chert. Triassic aged, neritic, dolomitic limestone blocks occur as olistoliths in this matrix. Low grade metamorphism, probably related to tectonics during the closure

of the ocean, can be seen in the lower levels of the accretional prism (Yazıcıgil, 2008).

Neogene units cover all of the sequence with an unconformity. They are represented by two groups; Miocene rocks and Pliocene rocks (Ağartan, 2010). The Miocene rocks in the study area are laterites. The Late Cretaceous aged serpentinized ultrabasic rocks were influenced by tropical-subtropical climatic conditions which dominated the western Anatolia during Miocene, leading to the formation of laterites. Consequently; these rocks were exposed to extreme physical and chemical weathering. This way, relatively mobile elements like Ni, Co, and Mn were leached and re-deposited at depths in the profile, while stable elements such as Fe and Al concentrated in the upper part of the profile, in the form of oxides and hydrated oxides. They formed a duricrust protecting the laterite from erosion.

Pliocene rocks in the area are represented with mostly detritic, lacustrine and fluvial sediments; named as Kanlıtepe Formation. There is an angular unconformity between the Kanlıtepe Formation and the underlying older rock units. Sediments are preserved as patches due to physical weathering.

Alluvium is seen at low lands in south of the study area and occupies the entire plain of Gediz River. This Quaternary alluvium consists of clay, silt, sand and gravels and unconformably overlies the older units (Yazıcıgil, 2008).

CHAPTER 3

HYDROGEOLOGY

3.1 Water Resources

The study area is located within the central part of the Gediz River's 17,118 km^2 catchment area. Gediz River forms the southern boundary of the model area and flows towards west to the Aegean coast, discharging through the Gediz Delta in the outer part of İzmir Bay. In the study area no surface water reservoir or lake is located; Gölmarmara Lake lies about 19 km and Demirköprü Dam is about 50 km east of the area.

3.1.1 Surface Water Resources

Gediz River, forming the southern boundary of the study area, is the major water resource within the study area. It flows in an E-W direction, and receives discharge from numerous creeks. Drainage pattern and major surface waters of the area are displayed in Figure 15.
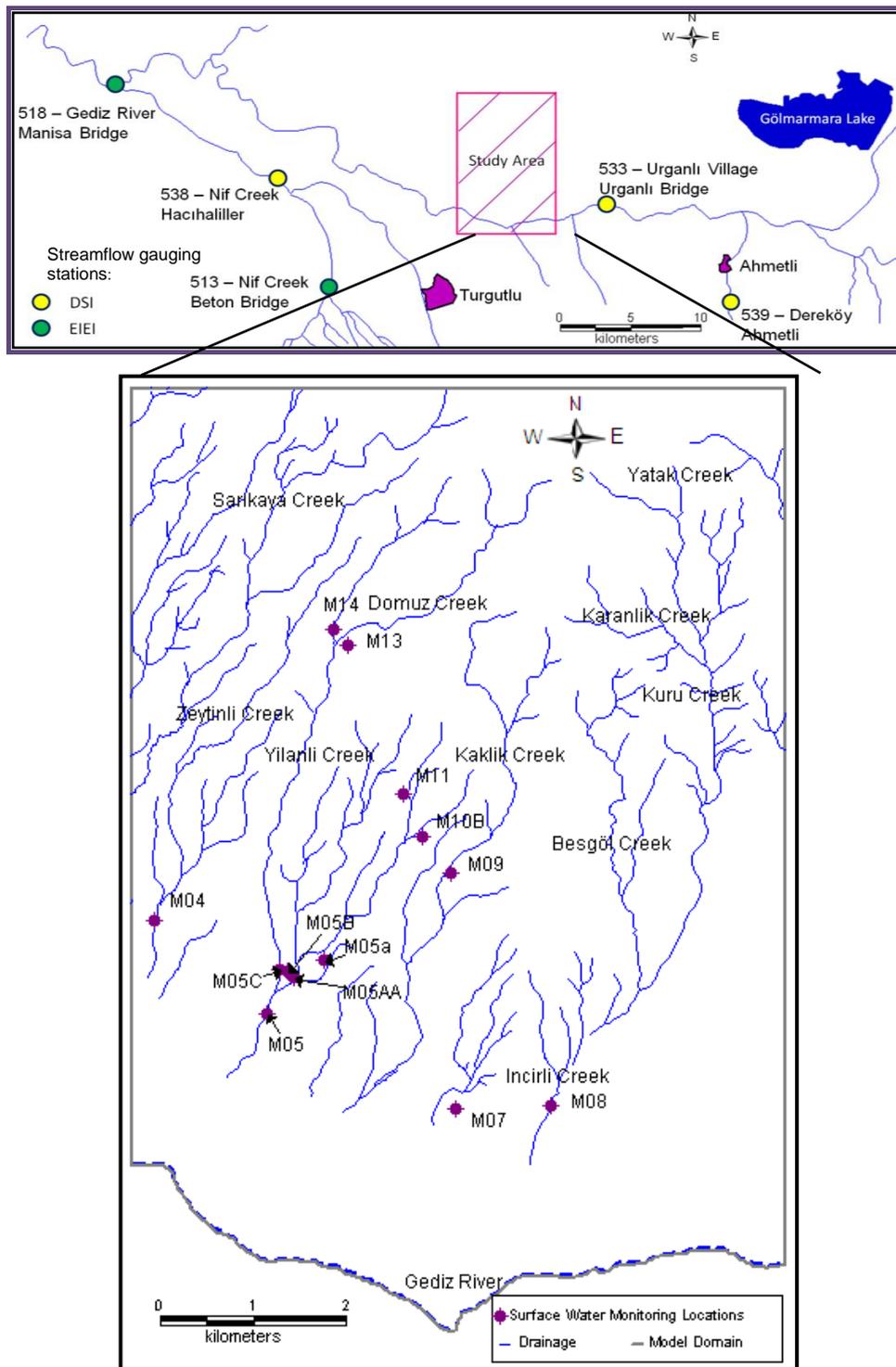
Figure 15 Drainage patterns, major surface waters, surface water monitoring stations and streamflow gauging stations in the region

In the study area, there are 13 surface water monitoring stations established by the company owning the operating licence of the mine. The locations of these monitoring stations together with the drainage pattern are also given in Figure 15. Due to the short observation period and lack of data, Soil Conservation Service (SCS) curve number method was used in the calculation of runoff from the project area sub-watersheds. Soil Conservation Service (1964) runoff estimates assume a relationship between accumulated total storm rainfall P, runoff Q, and infiltration plus initial abstraction (F+I_a). It is assumed that F/S=Q/P. Where F is infiltration after the beginning of runoff, S is potential abstraction, Q is direct runoff in inches, and P_e is effective storm runoff (P-I_a). With F = (P_e-Q) and P_e = (P-I_a) = (P-0.2S); based on data from small watersheds, Q = (P-0.2S)^2/(P+0.8S).

The SCS method uses the runoff curve number CN, related to potential abstraction by CN = 1000/(S+10), S being in inches. Thus, runoff curve numbers (CNs) indicate the runoff potential from a hydrologic soil-cover complex during periods when the soil is not frozen. A higher CN indicates a higher runoff potential. Runoff curve numbers vary as a function of land use, cover, and hydrologic soil groups. Hydrologic soil groups are divided into four types: A, B, C, and D. Hydrologic soil group A is sandy and well drained, group B is sandy loam, group C is clay loam or shallow sandy loam, and group D is heavy plastic clay that swells when wet. Group D is a poorly drained soil. Using satellite image and forestry maps with hydrologic soil group C, a weighted CN is calculated for each sub-watershed based upon the percent of area covered by various types of covers. The calculated CNs for sub-watersheds varied from a minimum of 75.1 to a maximum of 82.3 as

displayed in Table 4. The weighted CN value for the study area is 77 (Yazıcıgil, 2008).

Table 4 Runoff curve number calculation

Subwatershed No	Cover	CN	Area (%)	CNxArea (%)	Subwatwershed CN	Subwatershed Area (km²)	CN (%)
1	Wood-Good	70	22	1540	75.14	9.48	17.2
	Wood-Fair	73	28	2044			
	Wood-Poor	77	40	3080			
	Farm	85	10	850			
2	Wood-Good	70	30	2100	76.7	3.04	5.6
	Wood-Fair	73	25	1825			
	Wood-Poor	77	10	770			
	Farm	85	35	2975			
3	Wood-Good	70	30	2100	78.24	10.05	18.9
	Wood-Fair	73	24	1752			
	Dirtroad	87	1	87			
	Farm	85	35	2975			
	Baresoil	91	10	910			
4	Wood-Good	70	40	2800	75.96	5.14	9.4
	Wood-Fair	73	20	1460			
	Wood-Poor	77	15	1155			
	Dirtroad	87	1	87			
	Farm	85	15	1275			
	Baresoil	91	9	819			
5	Wood-Good	70	30	2100	82.26	2.28	4.5
	Dirtroad	87	1	87			
	Farm	85	40	3400			
	Baresoil	91	29	2639			
6	Wood-Good	70	25	1750	76.97	11.53	21.4
	Wood-Fair	73	30	2190			
	Wood-Poor	77	15	1155			
	Dirtroad	87	2	174			
	Farm	85	20	1700			
	Urban Development	91	5	455			
	Baresoil	91	3	273			
						41.52	77

Several streamflow gauging stations were established on the Gediz River and its tributaries by the State Hydraulic Works (DSİ) and Electrical Power

Resources Survey and Development Administration (EİEİ). Stations 518 and 533 are located downstream and upstream of the study area, respectively; and have been recording data for long periods (Figure 15). The streamflow gauging station 518 has been recording flow rates for approximately 40 years, while station 533 has been recording for 13 years.

The monthly river flow rates show the effect of winter rainfall and the controlled releases of discharges from Demirköprü Dam and the Gölmarmara Lake. The flow rates are higher in the winter and early spring (January through March) following the high amount of winter rainfall and then decrease through spring and early summer. It is natural that the flow rates are low in summer and fall months; however with the release of water from Demirköprü Dam and the Gölmarmara Lake, the rates are kept at a moderate level. Thus, as a result of DSI's control, the lowest river flows typically occur in May-June and September-October. Hence, the average monthly discharge at Station 518 varies from a maximum value of 86.8 m^3/s in February to a minimum value of 19.46 m^3/s in June; the average annual being equal to 42.5 m^3/s. The average monthly discharge at Station 533 varies from a maximum value of 22,45 m^3/s in February to a minimum value of 4.88 m^3/s in September; the average annual being equal to 12.7 m^3/s (Yazıcıgil, 2008). Related graph about average monthly flow is displayed in Figure 16.

	Oct	Nov	Dec	Jan	Feb	Mar	Apr	May	Jun	Jul	Aug	Sep
Station No 518	21.4	25.06	48.59	74.58	86.8	75.56	54.74	33.73	19.46	23.46	25.6	22.23
Station No 533	8.63	9.44	12.95	21.22	22.45	17.65	13.62	8.17	5.02	14.93	13.4	4.88
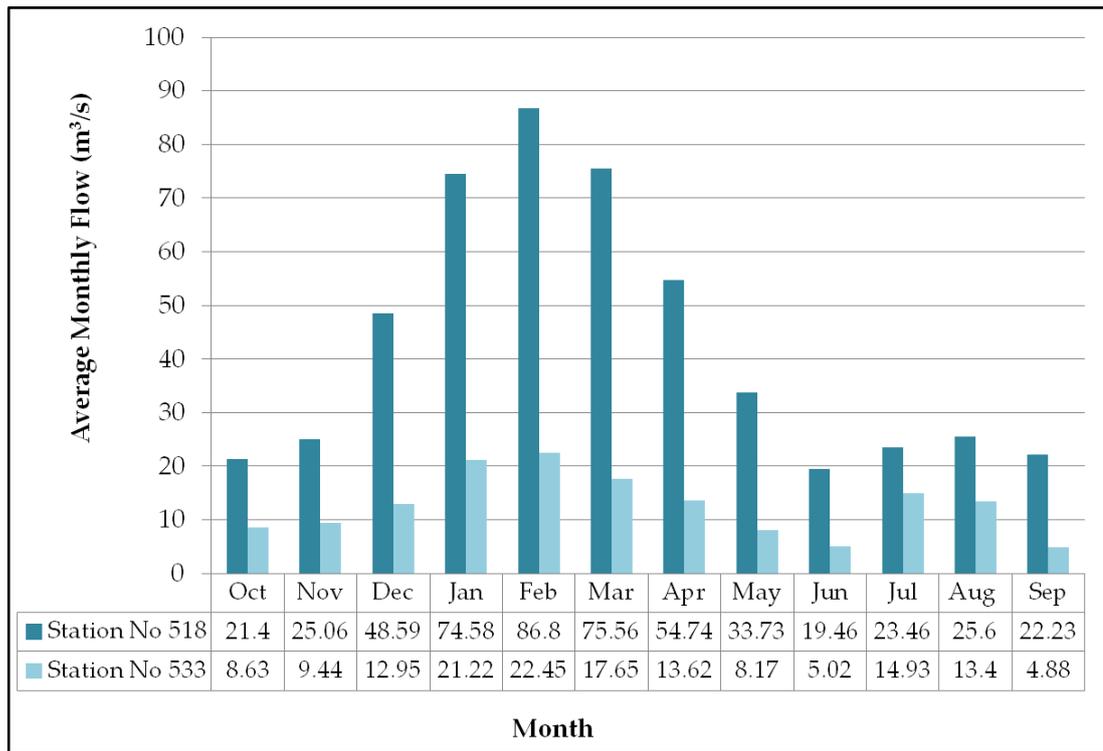
Figure 16 Average monthly flow rates at Stations No. 518 and 533

3.1.2 Springs and Seeps

In the study area, six springs and two seeps are located along the valleys of the ephemeral creeks (Figure 17). As seen in Table 5, the discharge rates are minor (Yazıcıgil, 2008). The total average spring discharge is less than 0.4 L/s; which is ignorable in our study. With the exception of SP-3, the water of which is transported to a fountain in the Temrek Village, none is used as a source of water supply for the nearby communities.
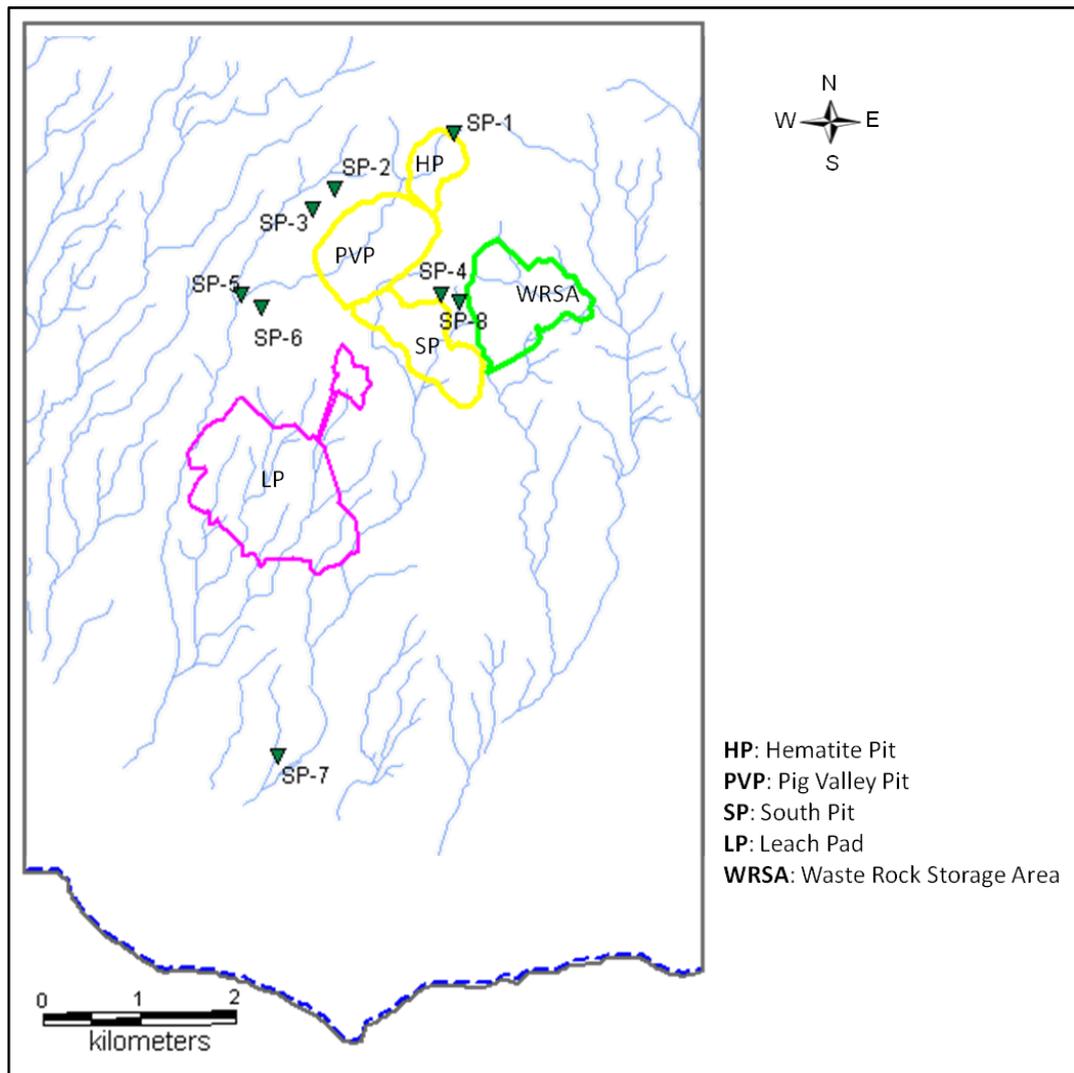
Figure 17 Springs and seeps in the study area

Table 5 Discharge rates of springs

Spring	Coordinates		Elevation (m)	Unit	Average Discharge (L/s)
	Easting	Northing			
SP-1	567442	4275846	946	Kanlıtepe Formation	0.14
SP-2	566205	4275293	665	Ultramafic Rocks	0.05
SP-3	565967	4275072	609	Ophiolitic Melange	0.05
SP-6	565451	4275066	395	Ultramafic Rocks	0.06
SP-7	565620	4269434	90	Kanlıtepe Formation	0.02
SP-8	567490	4274105	715	Ultramafic Rocks	0.02

3.1.3 Wells

In the study area; there are 184 wells, all of which are drilled by individuals. All the wells located in the area are used for irrigational purposes (Figure 18).
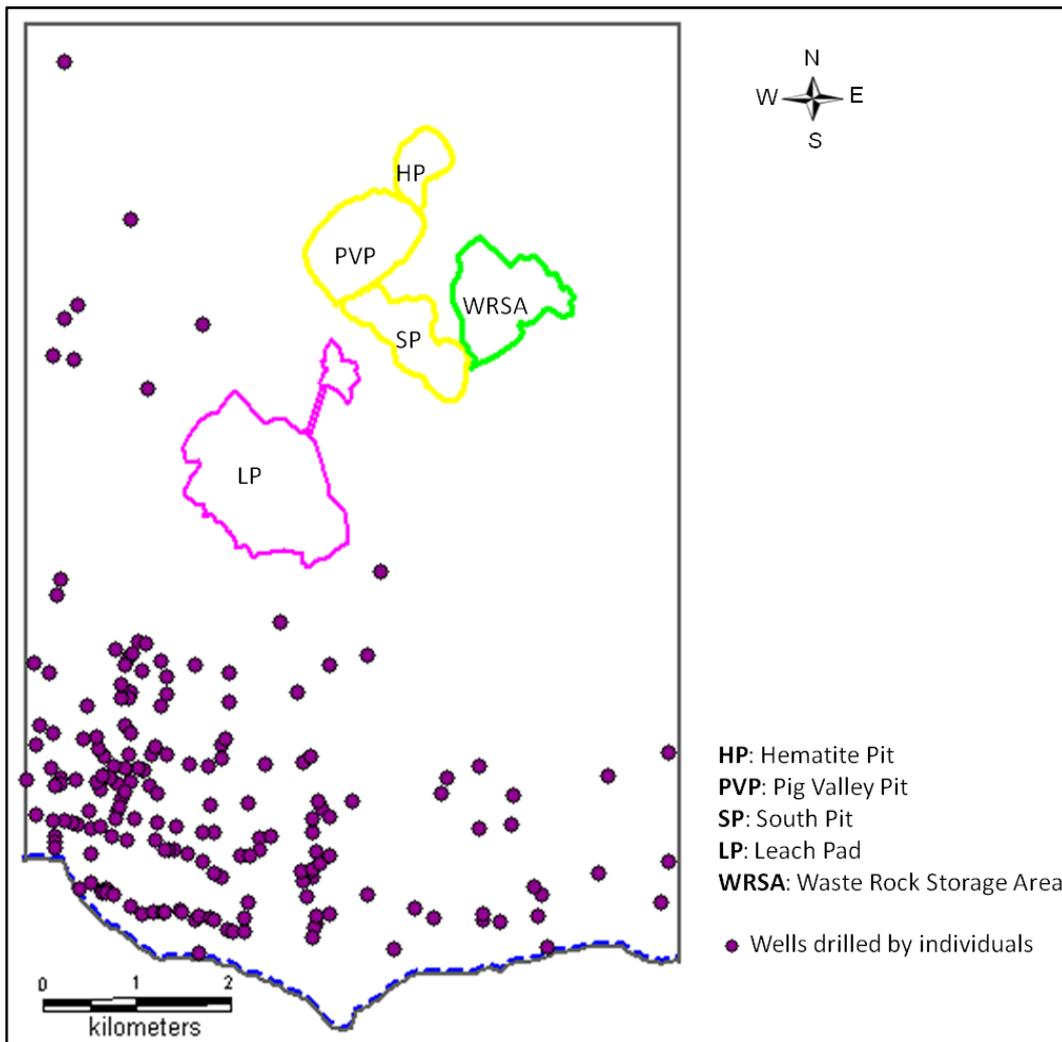
Figure 18 Wells located in the area

3.2 Groundwater Bearing Units

3.2.1 Hydrogeologic Classification of Groundwater Bearing Units

The principal aquifer of regional importance in the vicinity of study area is the Quaternary alluvium aquifer that occupies the plain areas along the Gediz River to the south of the area. It consists of a mixture of clay, silt, sand, gravel and boulders. The underlying sandstones, conglomerates and the limestones of the Kanlıtepe Formation also form a regional aquifer of secondary importance (Figure 19). These deposits are thickest in the central part of the valley, in the region of the Gediz River, and thin to the edges of the valley where they abut against the older rocks. Some of the project area and its vicinity are underlain by these Neogene age sedimentary deposits. The laterites and ultrabasic rocks belonging to the İzmir-Ankara Suture Zone have low permeability to render them as aquifers. The fractured sections of these formations may locally form perched aquifers to yield water to some ephemeral springs.
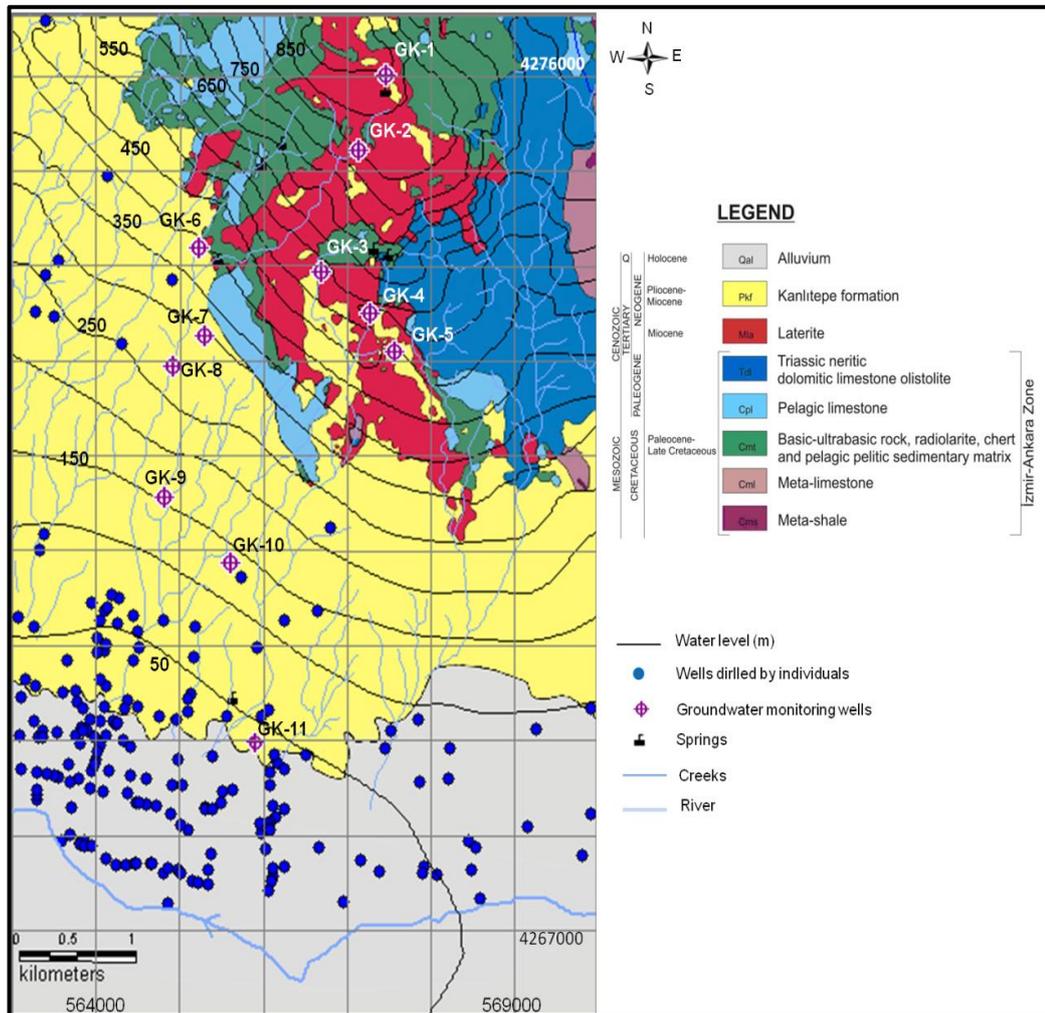
Figure 19 Hydrogeological map of the study area

3.2.2 Hydraulic Properties of Groundwater Bearing Units

There are 11 groundwater monitoring wells (GK-1 to GK-11) within the study area (Figure 19). Hydraulic conductivity and storativity values were obtained regarding the results of pumping tests conducted at these wells. In Table 6, detailed information about monitoring wells is given. Although

initially four wells were targeted in laterites, only one (GK-1) could be tested because GK-3, GK-4, and GK-5 were dry. The laterites in GK-1 has the highest hydraulic conductivity tested (2.89×10^{-6} m/s). The fault extending through the Pig Valley probably passes through the Hematite Pit and GK-1 and contributes to a relatively higher permeability by fracturing the rock units around GK-1. The hydraulic conductivity of ultramafic rocks were tested at two (GK-2 and GK-6) monitoring wells, both giving almost the same magnitude of hydraulic conductivity value of about 6.5×10^{-7} m/s. The hydraulic conductivity of Kanlıtepe formation, tested in four (GK-6, 7, 8, 9, and 11) wells varies from 1.16×10^{-8} m/s to 1.23×10^{-6} m/s, the geometric average being equal to 1.37×10^{-7} m/s. The variation in hydraulic conductivity of the Kanlıtepe formation is several orders of magnitude, indicating the highly heterogeneous nature of the formation. Table 7 summarizes the hydraulic parameters calculated from pumping tests. In the study area, there are no monitoring wells drilled into the alluvium; thus for the hydraulic conductivity of alluvium, data from a study of the whole Gediz River Basin was used (Ağartan, 2010). Consequently, hydraulic conductivity of alluvium is 4.6×10^{-5} m/s.

Table 6 Information about monitoring wells

Well Name	Easting (m)	Northing (m)	Ground Elevation (m)	Borehole Depth (m)	Depth to Water (m)	Target Formation
GK-01	567470	4276017	956.23	100	57.03	Laterite
GK-02	567143	4275220	820.84	62.5	19.68	Ultramafic Rocks
GK-03	566700	4273940	615.02	85	-	Laterite
GK-04	567269.5	4273507	558.37	81	-	Laterite
GK-05	567571	4273103	583.38	140	-	Laterite
GK-06	565235.3	4274199	390.36	75	Artesian	Ultramafic Rocks
GK-07	565298.6	4273260	358.48	207	76.15	Kanlıtepe Formation
GK-08	564917	4272951	284.65	86	27.33	Kanlıtepe Formation
GK-09	564825	4271561	178.28	90	28.76	Kanlıtepe Formation
GK-10	565613	4270882	188.75	84	47.51	Kanlıtepe Formation
GK-11	565925.6	4268971	85.39	112	40.6	Kanlıtepe Formation

Table 7 Summary of hydraulic conductivity and storativity parameters

	Hydraulic Conductivity (m/s)				Storativity	
	K (min)	K (max)	K (Arithmetic Average)	K (Geometric Average)	S (min)	S (max)
Laterite	-	-	2.89E-06	-	0.148	
Ultramafic	5.58E-07	7.43E-07	6.50E-07	-	0.033	
Kanlıtepe Formation	1.16E-08	1.23E-06	4.63E-07	1.37E-07	0.01	0.22

The calculated storativities are generally low (0.02), except at GK-1 and GK-9 where they are high (0.15-0.22). The higher values noted at these wells may have been produced by the fracturing and faulting that affects them. Both of them are located on probable faults.

3.2.3 Groundwater Levels

3.2.3.1 Spatial Variation in Groundwater Levels

Using spring elevation data and available groundwater level data from monitoring wells, a groundwater elevation map was developed. The elevations of the springs located in the western part of the project area (SP-2, SP-3, SP-5 and SP-6) were conformable with the regional groundwater levels; however elevations of the springs located in the north and east of the area

(SP-1, SP-4 and SP-8) were significantly above the regional water table contours. Hence, these three springs are probably discharging from a local perched aquifer.

Groundwater flow in the study area is from N-NE toward S-SW as shown in the groundwater level map in Figure 20. Groundwater levels decrease from about 900 m in the north to 50 m in the south along the Gediz River. Thus, the northern boundary where Çaldağ is located forms a recharge boundary. The Gediz River located in the south, forms a drainage boundary where most of the discharge takes place. The hydraulic gradient is relatively higher (about 0.2) in the northern part of the area where laterites and ultramafic rocks crop out and it is lower (0.10 to 0.06) at the southern part of the area where Kanlıtepe Formation crops out. Lower gradients at the southern part correspond to the relatively thicker and permeable Kanlıtepe Formation (Yazıcıgil, 2008). Additionally, depth to water table map is given in Figure 21.

The evaluation of groundwater levels indicate that the deeper parts of the planned pits will encounter a standing water level which have to be lowered by dewatering to permit dry working conditions. In Part 1.3, Figures 4, 5 and 6; this was explained in more detail.
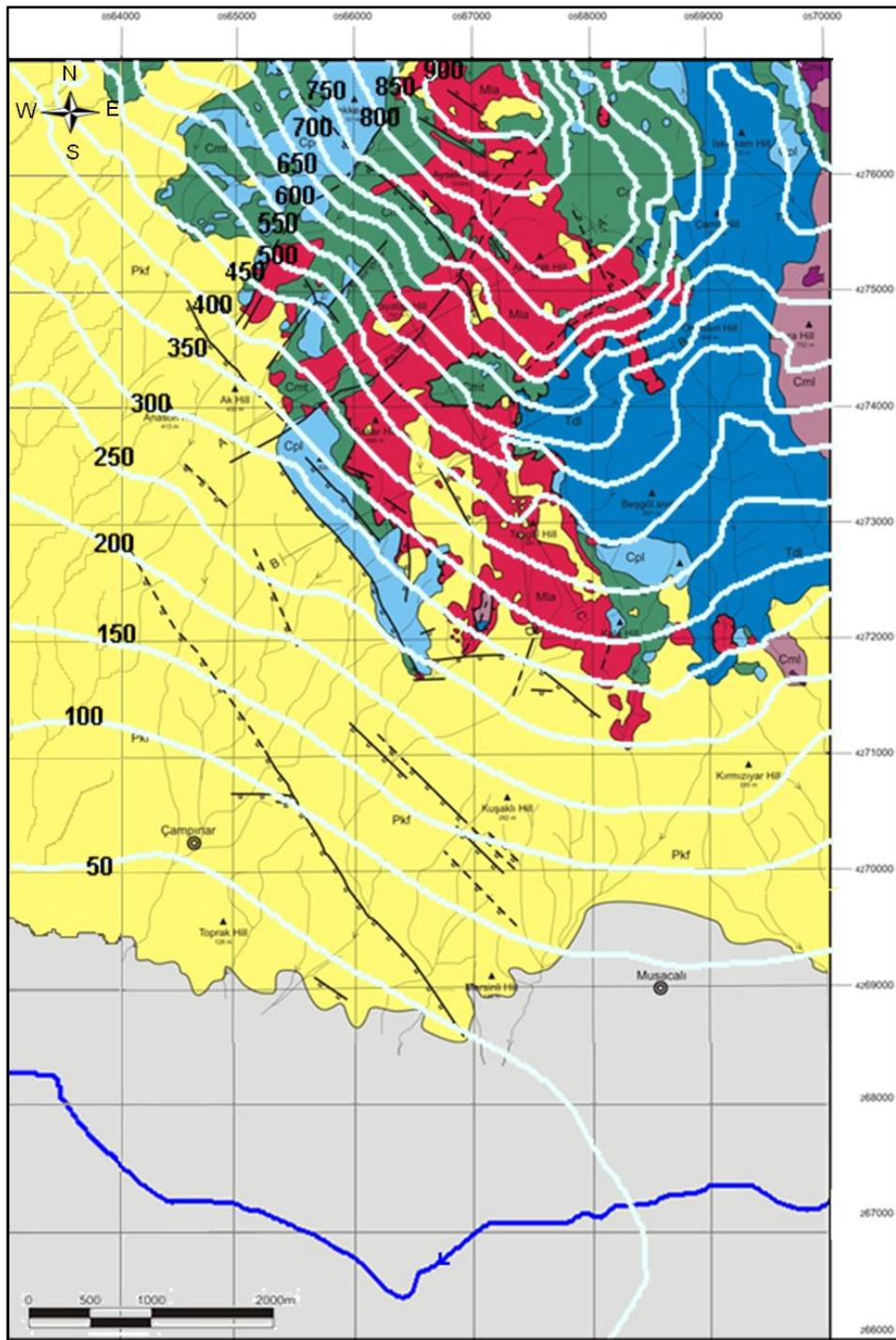
Figure 20 Groundwater level map of the study area
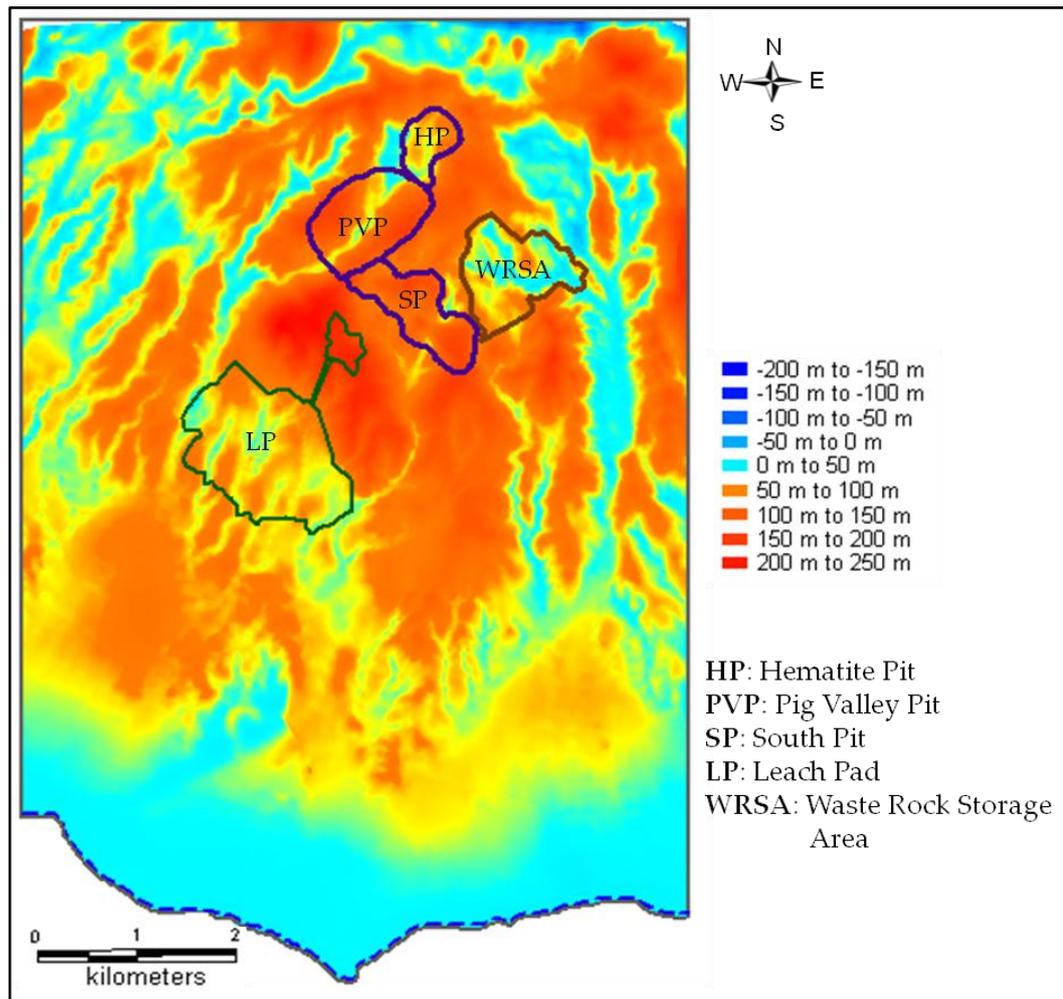
Figure 21 Map of depth to water table

3.2.3.2 Temporal Changes in Groundwater Levels

In the groundwater monitoring wells mentioned in Part 3.2.2, water levels are measured since 2008. The most recent measurement is 14.09.2011 dated. The target formations of these wells (as previously displayed in Table 6) are laterite for GK-1, ultramafic units for GK-2 and 6, and Kanlıtepe Formation for GK-7, 8, 9, 10 and 1in Part 3.2.2 displays the locations of these wells.

51

Figure 22Figures 22, 23, 24, 25, 26, 27 and 28 display the temporal water level changes in monitoring wells. Examination of Figure 22 and 23 together, shows that the rise in water levels corresponds to February and decrease starts in June and May in GK-1 and GK-2, respectively. It can be concluded that GK-1 and GK-2, which are the northernmost located monitoring wells in the area, display seasonal fluctuations. In other wells, these fluctuations are not observed. The maximum change in the groundwater levels, which is 9.5 m, is observed in GK-2.
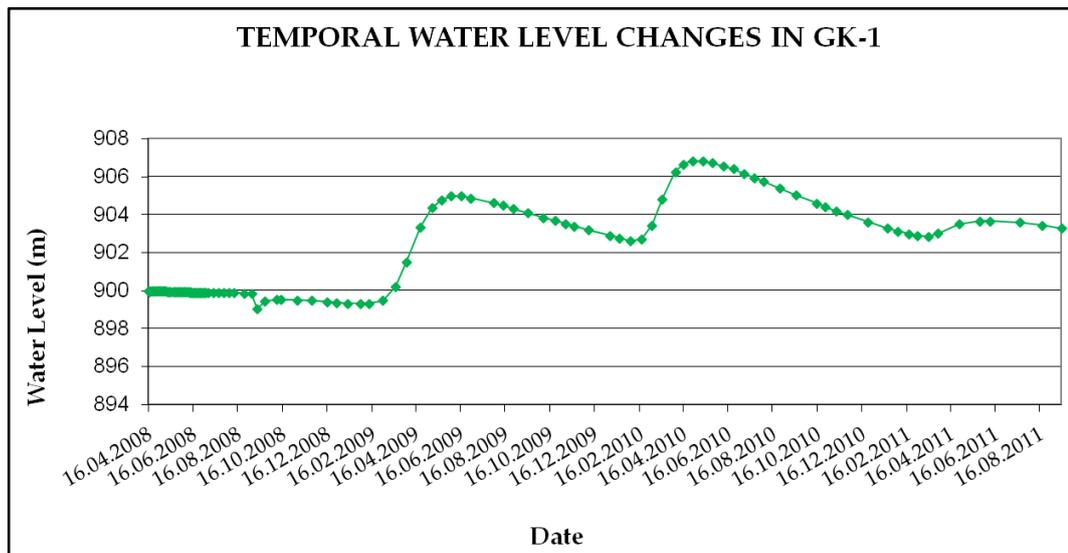
Figure 22 Temporal water level changes in monitoring well GK-1
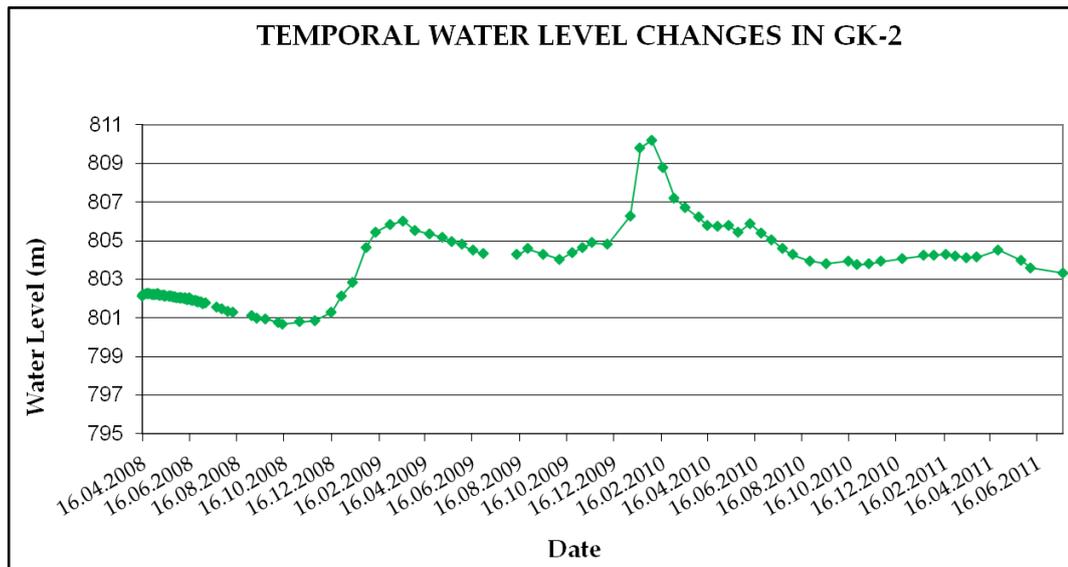
Figure 23 Temporal water level changes in monitoring well GK-2
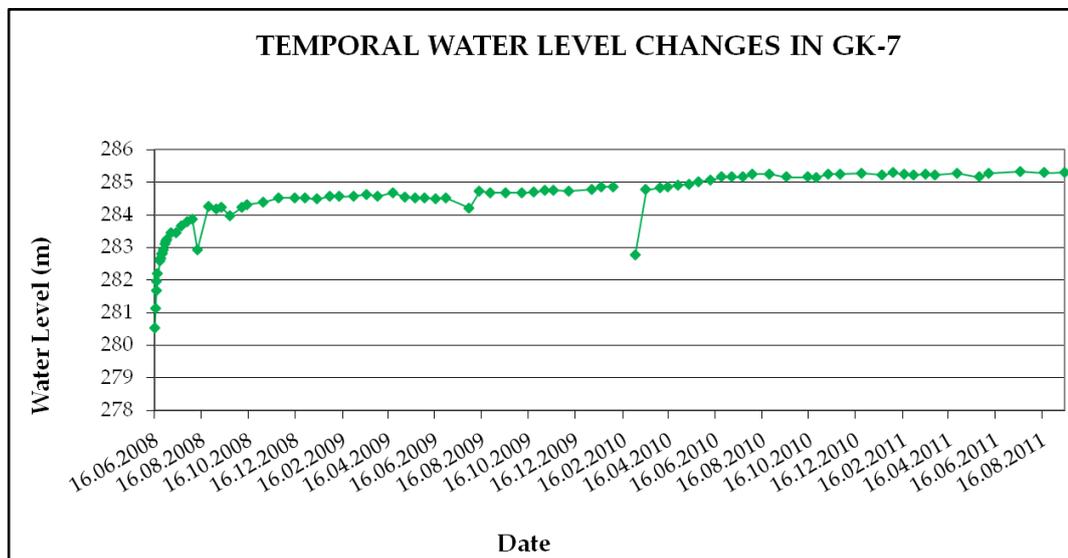
Figure 24 Temporal water level changes in monitoring well GK-7
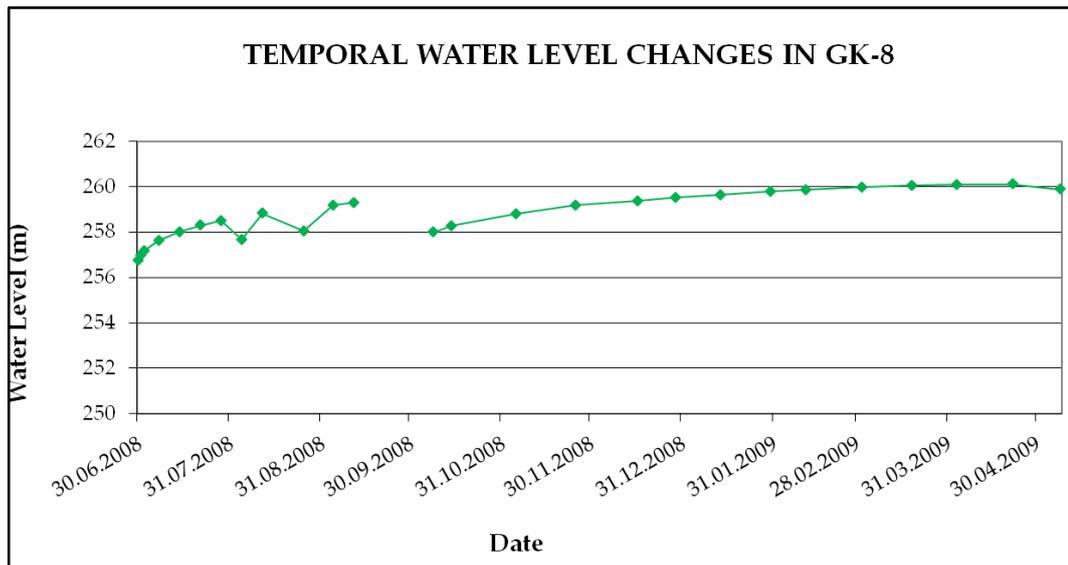
Figure 25 Temporal water level changes in monitoring well GK-8
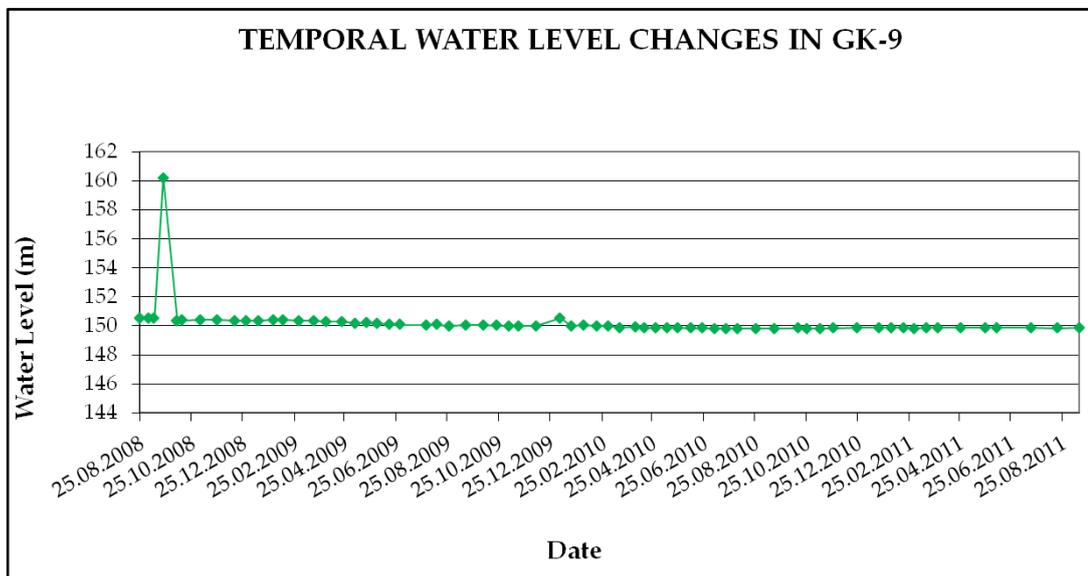
**Figure 26** Temporal water level changes in monitoring well GK-9
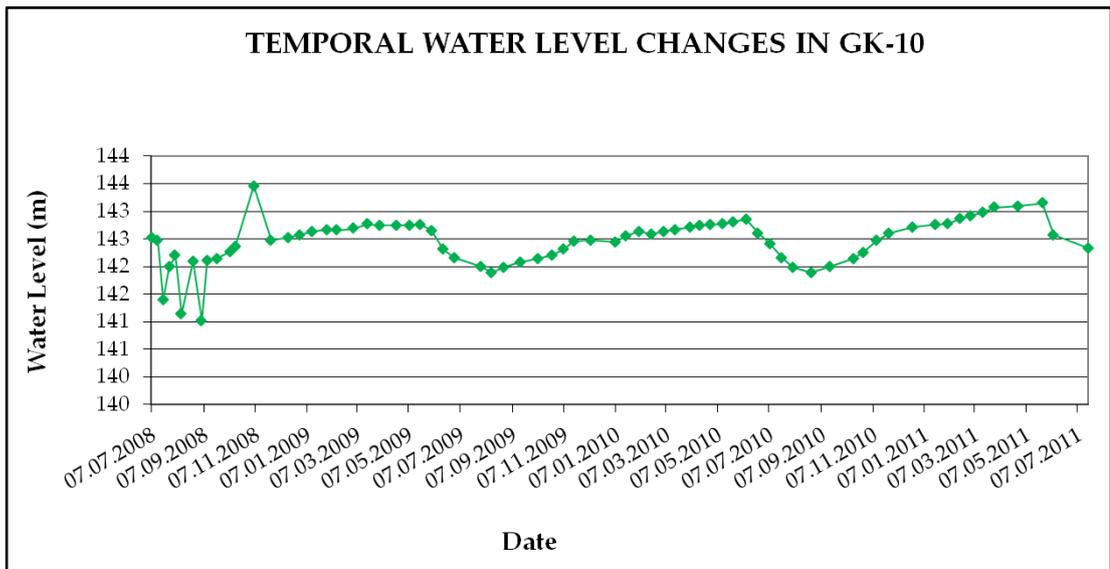
Figure 27 Temporal water level changes in monitoring well GK-10
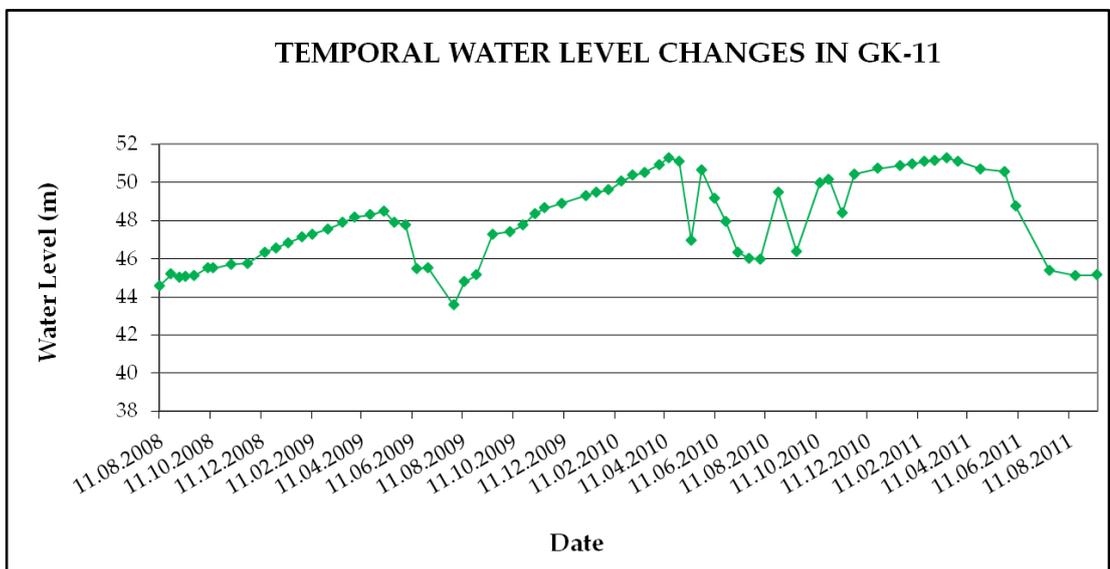
Figure 28 Temporal water level changes in monitoring well GK-11

3.2.4 Water Balance and Groundwater Recharge

As mentioned before; using SCS curve number method, runoff was calculated as 140.4 mm/yr. In order to calculate potential evapotranspiration, Thornthwaite method was used. In the water balance equations, the long-term average monthly temperature and average monthly precipitation values for Turgutlu meteorological station were used. Initial soil moisture value is assumed as 100 mm. The results of water balance calculations are summarized in Table 8. The results show that, 61.4% of the annual precipitation is lost into the atmosphere as actual evapotranspiration, 27.8 % runs off, and 10.8 % percolates into the ground to recharge the groundwater system.

Table 8 Annual Water Balance Results for the Project Area

	Annual Amount (mm)	**Proportion of Annual Rainfall (%)**
Precipitation	505.3	100
Evapotranspiration	310.3	61.4
Runoff	140.4	27.8
Percolation	54.6	10.8

CHAPTER 4

GROUNDWATER FLOW MODEL

4.1 Software Description

Modular finite difference groundwater flow model, MODFLOW-2000 code developed by the United States Geological Survey (USGS) was used in this study (Harbaugh et al., 2000). The groundwater model in the study was developed using Visual MODFLOW 2010.1, which is a graphical interface for MODFLOW. In Visual MODFLOW; MODFLOW, MODFLOW-SURFACT, MT3DMS, SEAWAT and ZONEBUDGET can be integrated.

Since 1980s, MODFLOW is continuously being developed with new packages and tools. Worldwide, it is widely used in groundwater flow modeling. Selection of this software in this study was based on these specifications:

- It can simulate regional models, and visualize the results using 2D or 3D graphics,
- It is capable of simulating a wide variety of hydrogeologic processes in field conditions and various geological features,
- It can simulate confined, unconfined and leaky aquifers under both steady-state and transient conditions.

4.2 Conceptual Model

As explained in part 3.2.1, main aquifer of regional importance is the alluvium aquifer that occupies the plain areas in the south. The underlying Kanlıtepe Formation also forms a regional aquifer of secondary importance. The laterites and ultrabasic rocks of İzmir-Ankara Suture Zone have low permeability to render them as aquifers but fractured sections of these formations have high hydraulic conductivity. Conceptual model development is the main step of modeling, thus detailed examination of the system is necessary. Since the model area is complex and rapid changes in elevation occur in short distances, it is important to simulate the heterogeneity in detail, both by horizontal and vertical means. This is achieved by means of fine grid cell sizes and large number of layers. Considering the main purpose of the study, which is the determination of dewatering requirements for the mine, the deepest pit bottom elevations were evaluated for the thickness of first layer. Bottom of the first layer is assigned to be below the deepest pit bottom elevation. The underlying three layers have varying thicknesses and the bottom lowermost layer is at -600 m. Figure 29 is a N-S directional cross section showing the modeled layers.
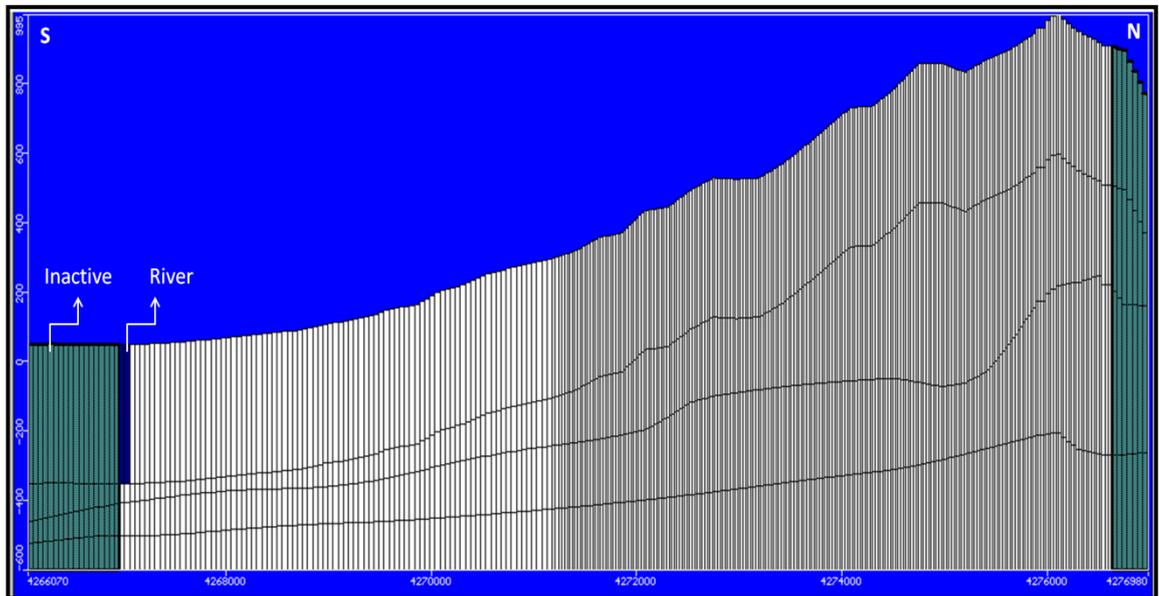
Figure 29 N-S cross section displaying four model layers

In the conceptual model, the first layer is composed of four different units depending on different hydraulic conductivities: Alluvium, Kanlıtepe Formation, laterites and rocks belonging to İzmir-Ankara Suture Zone. Downwards, each layer also constitutes four units. During calibration, this grouping was changed and number of units in each layer increased.

4.3 Model Setup

4.3.1 Finite Difference Grid

Gridding is obligatory in order to define and discretize the domain. To be able to obtain a reasonable solution time, the minimum number of grids that will best display the boundaries and heterogeneity of the aquifer should be

selected. The grid size is selected to be 50 m in both rows and columns, and is refined to 25 m (in both directions) in areas where the three open pits, leach pad area and waste rock storage area are located. 25 m grid size was also chosen for the area close to the northern model boundary since heads in this area display abrupt changes in short distances and it is important to correctly simulate this complexity. The gridded model domain is displayed in Figure 30.
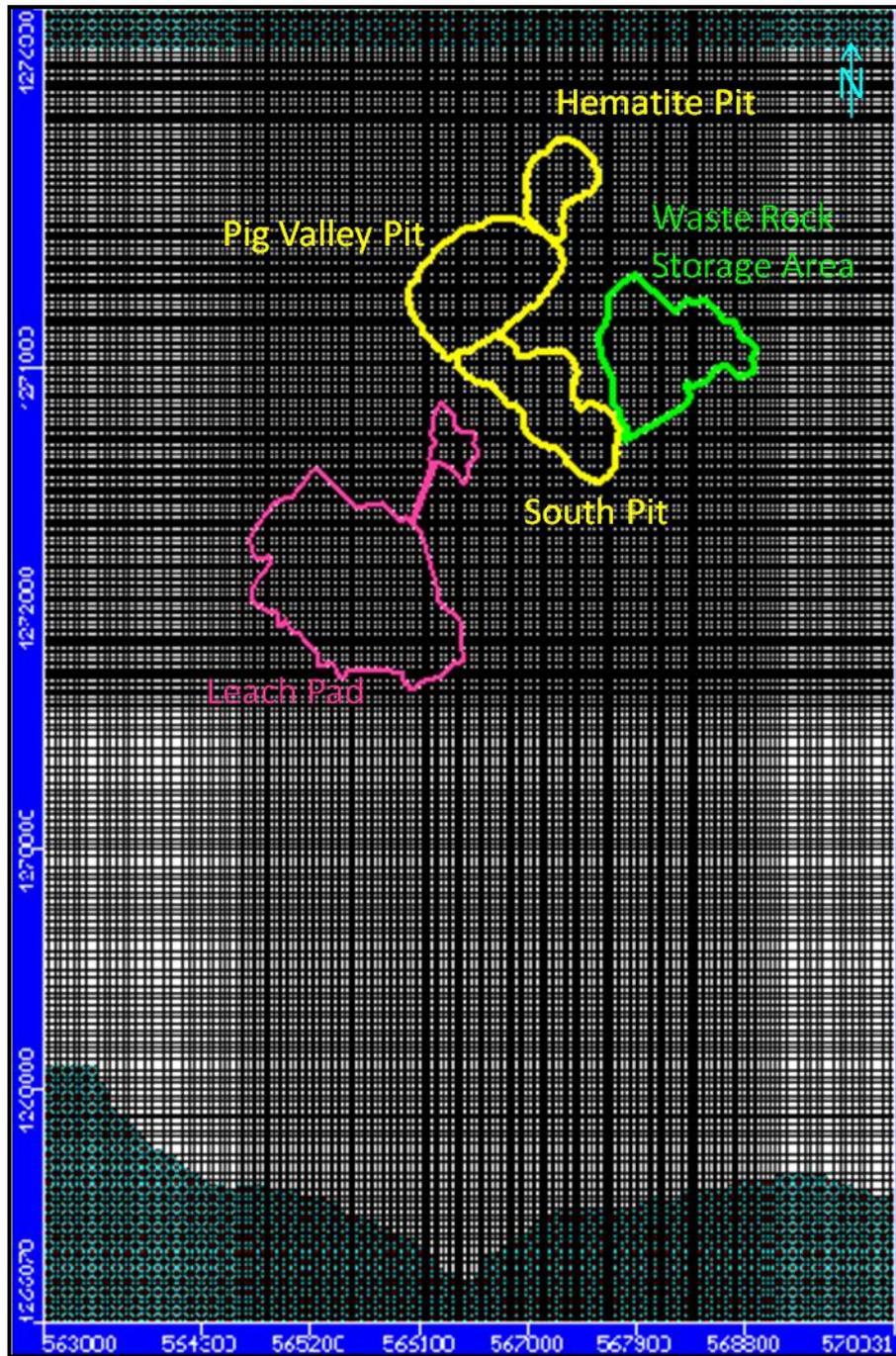
Figure 30 Gridded model domain

4.3.2 Boundary Conditions

In the case of a groundwater flow model, boundary conditions describe the exchange of flow between the model and the external system. Geological and hydrogeological characteristics of the area are mainly considered in determination of model boundaries. As mentioned and displayed before (Figure 20), flow direction in the study area is from northeast to southwest. Thus, to simulate the continuous inflow to the model domain from the northern boundary, general head boundary condition was assigned to this portion. Similarly; in order to simulate the outflow of water from the system in the northwestern part, general head boundary condition was assigned to this part as well. While assigning general head boundary condition, the boundary head was obtained from topography corresponding to the selected cells. Boundary distance was taken as 100 m and conductance was automatically calculated by the software via default conductance formula.

Gediz River flows along the southern boundary of the model domain, so it was simulated with river package. While assigning the river, river stage elevation was assigned to be 5 m below the corresponding topography in river cells, river bottom elevation to be 0.5 m below the stage and riverbed thickness to be 1m. Using the input parameters, the software calculated the conductance by default conductance formula.

Additionally, major creeks in the study area are modeled as drains. Drains remove water from the system as long as the water table is above specified drain elevation; otherwise, when the drain elevation is below water table, the drains have no effect. The drain package in MODFLOW is the most relevant

one for simulating seasonal water flow in a creek (Duru, 2004). In the model; the drain elevation was assigned to be 5 m below the topography and initially, the conductance was assigned as 1000 m^2/day for all the drains representing the creeks, during calibration this parameter was changed too. Finally, no flow boundary condition was used for the rest of the boundaries. In Figure 31, boundary conditions are displayed.

Figure 31 Boundary conditions

63
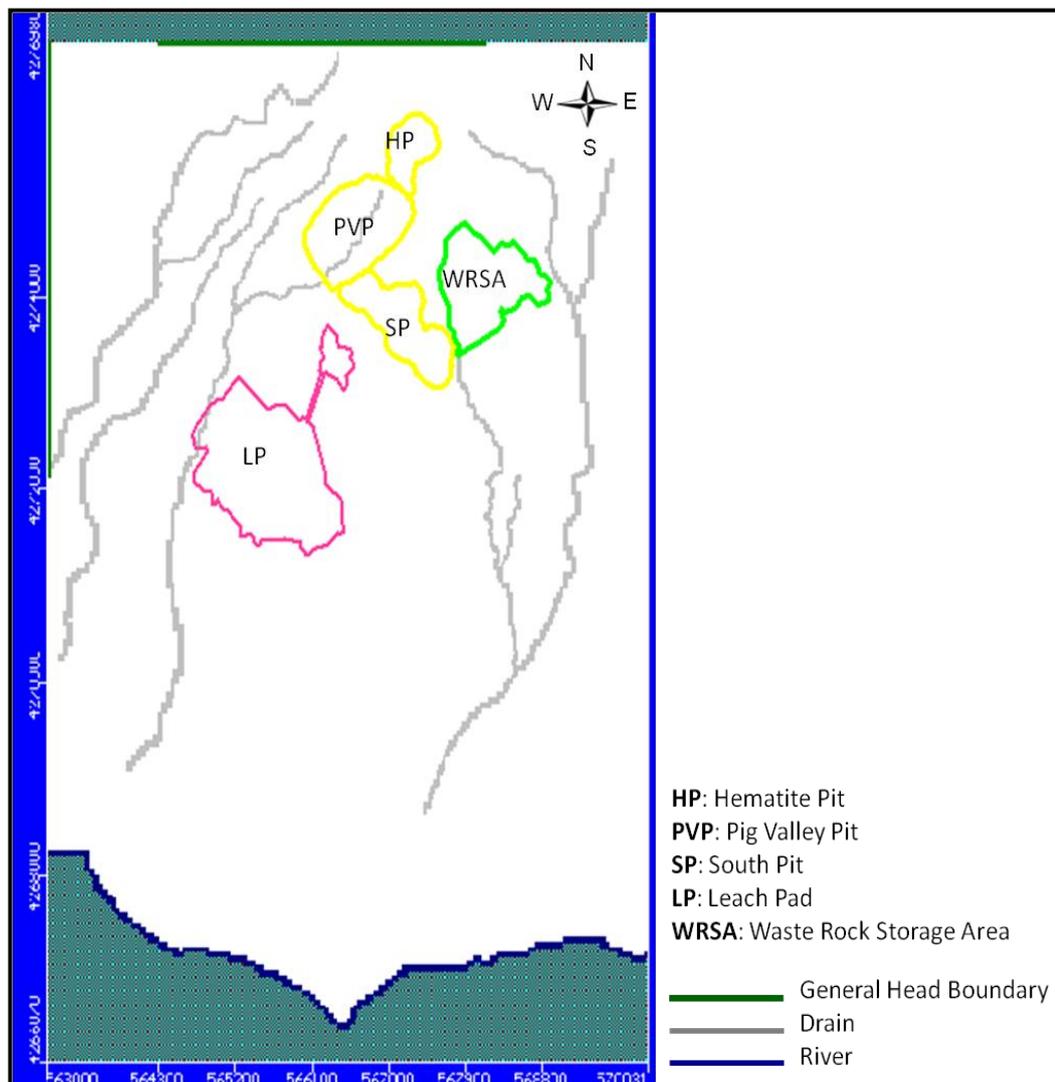
4.3.3 Hydraulic Parameters

As explained in part 4.2, at model setup 16 different hydraulic conductivity zones (4 zones for each of 4 layers) were defined. During calibration, number of zones was changed together with hydraulic conductivity values. Initially; in the first layer, the hydraulic conductivity values explained in part 4.2.2 were assigned. These are determined due to pumping tests. In second, third and fourth layers, hydraulic conductivity zones have the same spatial distributions but their numeric values are half of the upper one in each layer. Figure 32 displays the initial hydraulic conductivity distribution of first layer in plan-view. Also in Figure 33, the hydraulic conductivity zones assigned in conceptual model are shown on N-S directional cross section.
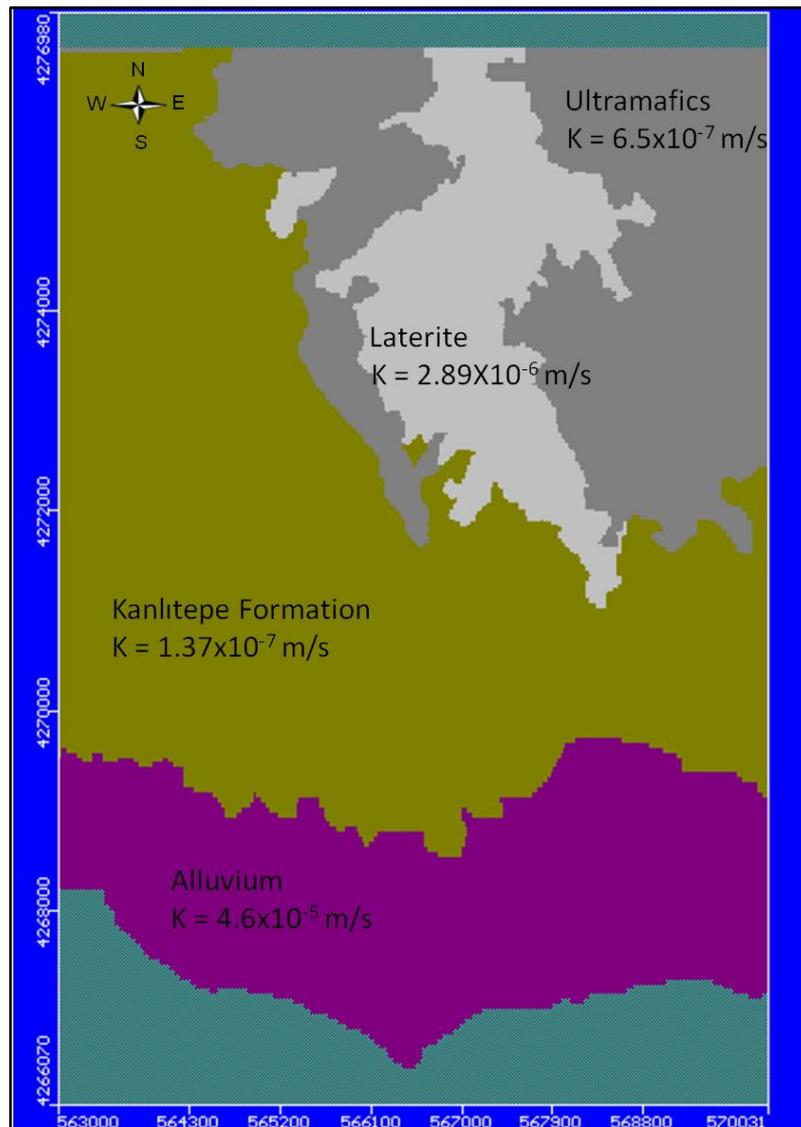
Figure 32 Hydraulic conductivity distribution of first layer in plan view in the conceptual model
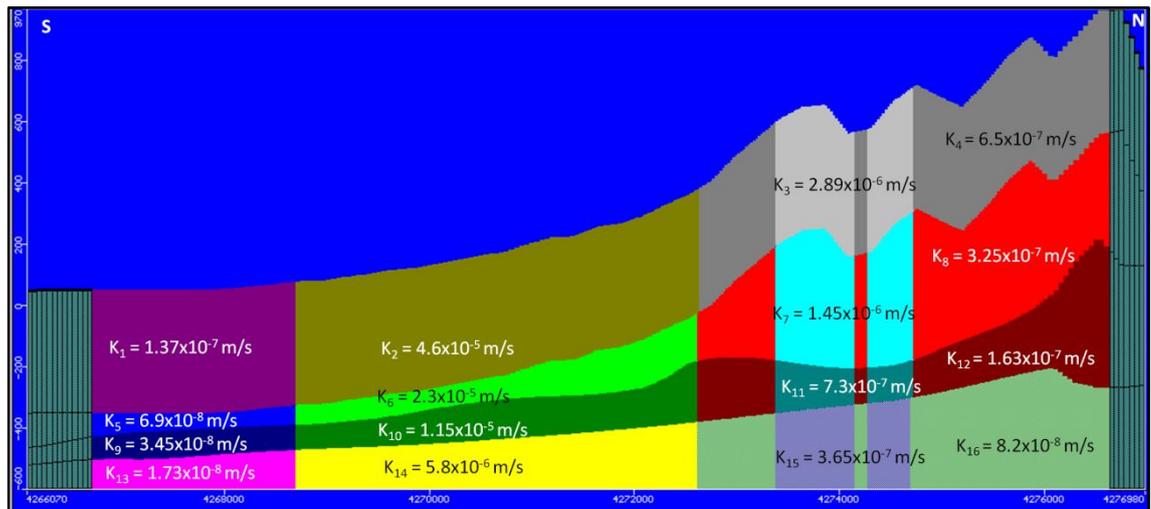
Figure 33 Hydraulic conductivity zones in the conceptual model, N-S directional cross section

4.3.4 Areal Recharge

Recharge from precipitation is the most important source for groundwater recharge, and as mentioned previously in part 3.2.4, it was calculated using Thornthwaite method. The calculated recharge value is 54.6 mm/yr but it was not assigned uniformly to the whole region. In the northeastern part where elevation is above 500 m; the recharge value was assigned to be 109.2 mm/yr (twice the calculated value). This is due to the fact that the elevation rises up to 1034 m and even snow is observed in these elevated areas, causing higher amounts of groundwater recharge than the rest of the region. Figure 34 displays the recharge distribution in the study area.
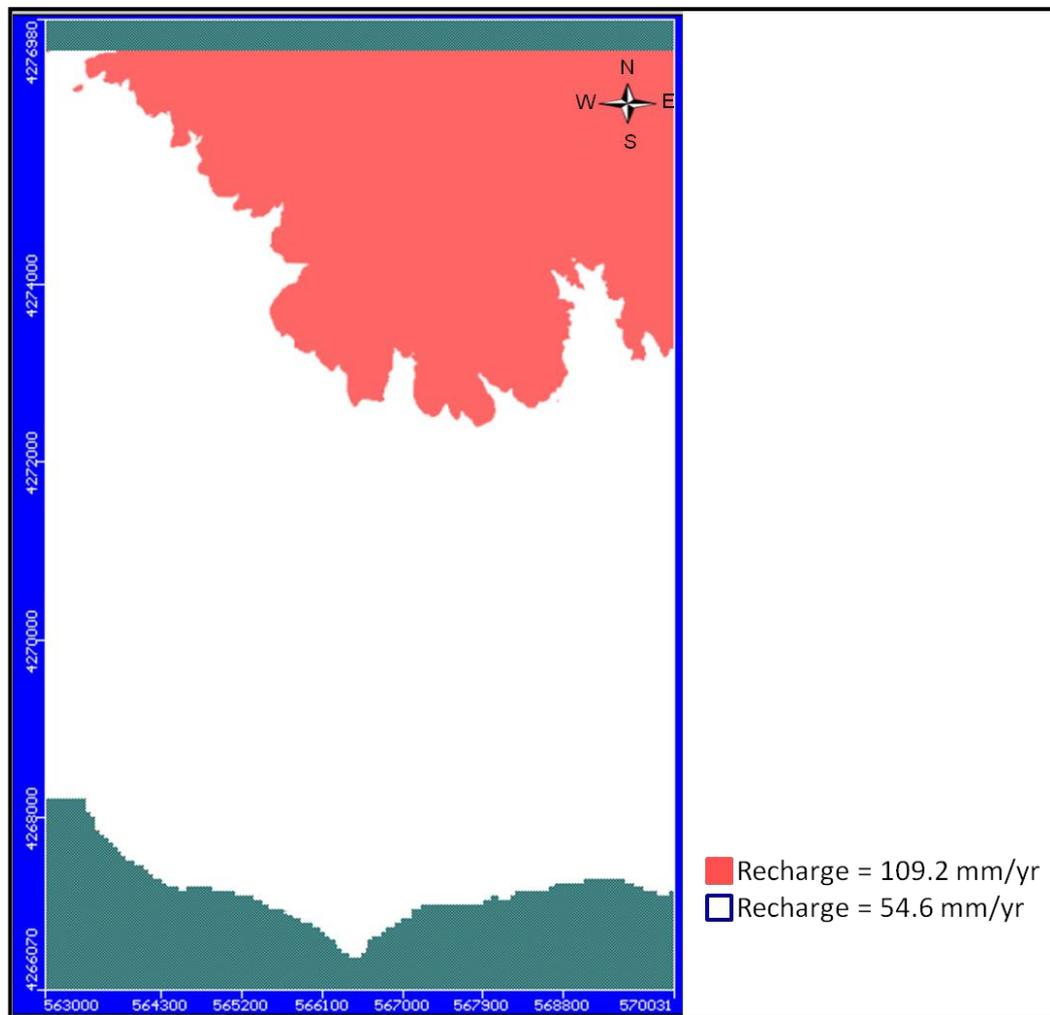
Figure 34 Recharge distribution in the study area

4.3.5 Wells

According to the DSI reports, water requirement of the area to be irrigated by wells was determined as 0.61 L/s/ha. It is assumed that pumping from the wells for irrigation purposes occur only in June, July, August and September. With the help of Google Earth, it was determined that the irrigation fields have an area of 2371 ha, requiring 14.995 hm³ of water annually. After this

calculation, discharges of the 172 wells introduced to the model were determined to be 238.86 m³ / day.

4.4 Model Calibration

4.4.1 RMS and Normalized RMS of the Calibrated Model

After the completion of model setup by introducing all the inputs to the software, calibration was carried out. In order to match the calculated groundwater levels with the observed ones; recharge, boundary conditions, hydraulic parameters and drain conductance values were adjusted within the limits of geology and hydrogeology.

One of the criteria in obtaining a satisfying match between calculated and observed heads is acquiring the minimum possible RMS (Root Mean Squared Error) or Normalized RMS. They are defined by Equations 1 and 2, respectively.

$$\text{RMS} = \sqrt{\frac{1}{n}\sum_{i=1}^{n}(h_{obs} - h_{cal})_i^2} \qquad (1)$$

$$\text{Normalized RMS (\%)} = \frac{\text{RMS}}{(h_{obs})_{max} - (h_{obs})_{min}} \qquad (2)$$

In these equations,

  n : total number of observation points,

  h_{obs} : observed groundwater level,

  h_{cal} : calculated groundwater level.

RMS is expressed in length units and Normalized RMS is expressed as percentage. The latter is a more representative measure of the fit, as it accounts for the scale of the potential range of data values. The aforementioned two values were calculated for all the wells located in the model area, and the calibration is achieved with a RMS of 39.194 m and a Normalized RMS of 4.569 %. The calibration graph is displayed in Figure 35. Considering the complexity of the region, this is a very successful fit; hence, it can be concluded that a good match between observed and calculated groundwater levels is obtained. Observed and calculated groundwater levels at the end of calibration are displayed in Figure 36.
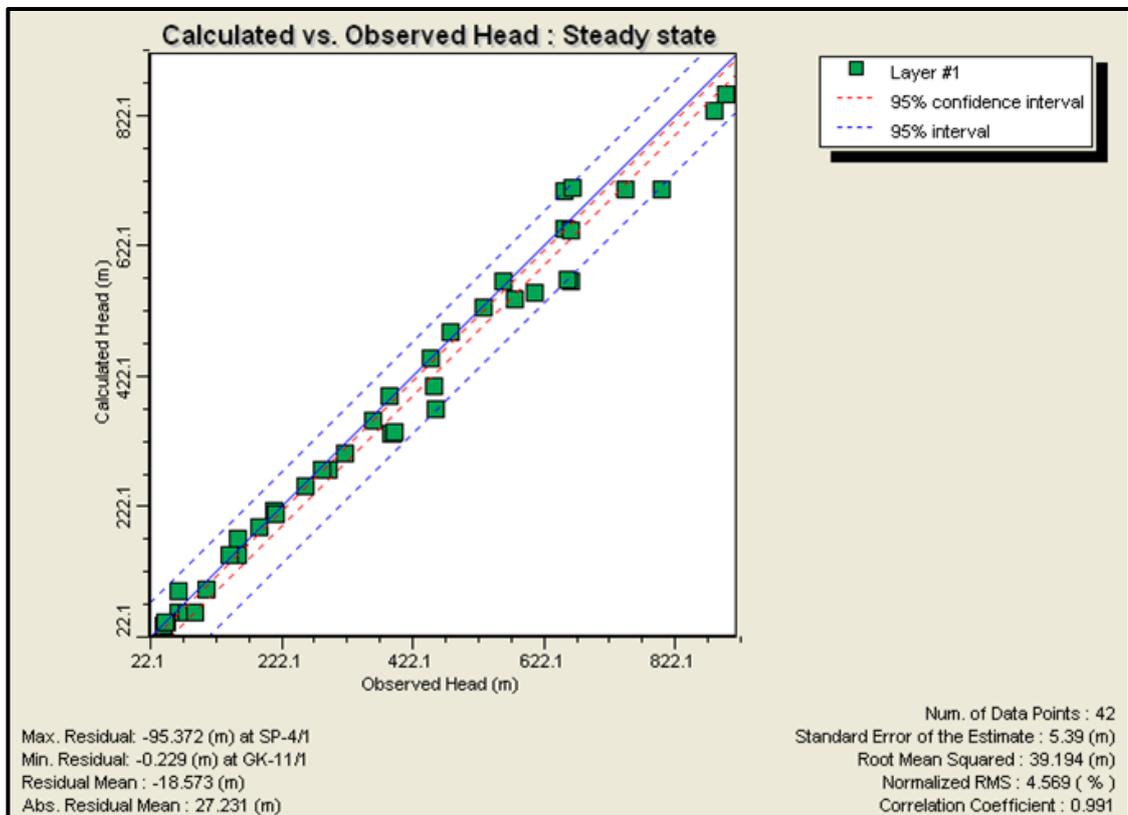
Figure 35 Calibration graph
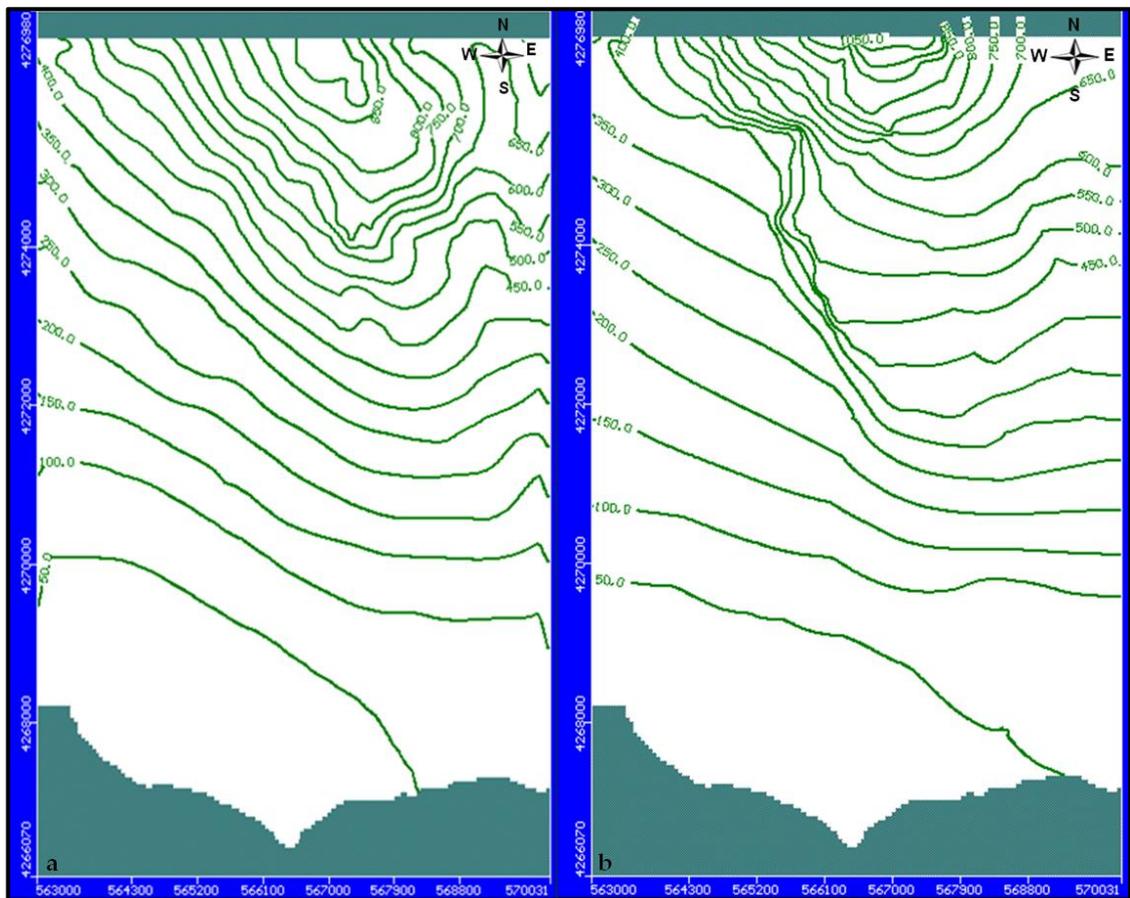
Figure 36 Observed heads (a) and calculated groundwater levels (b)

The new hydraulic conductivity distribution in the first layer after calibration can be seen in Figure 37. In the conceptual model, some units were grouped (ultramafic units and limestones) and assigned same hydraulic conductivity values. However, in the calibration step, regarding the comparison of calculated and observed heads, they were separated. As explained before; in layers 2, 3 and 4, hydraulic conductivities have same spatial distributions as the ones in the first layer but going downwards, each zone has a value half of the one above it.

70
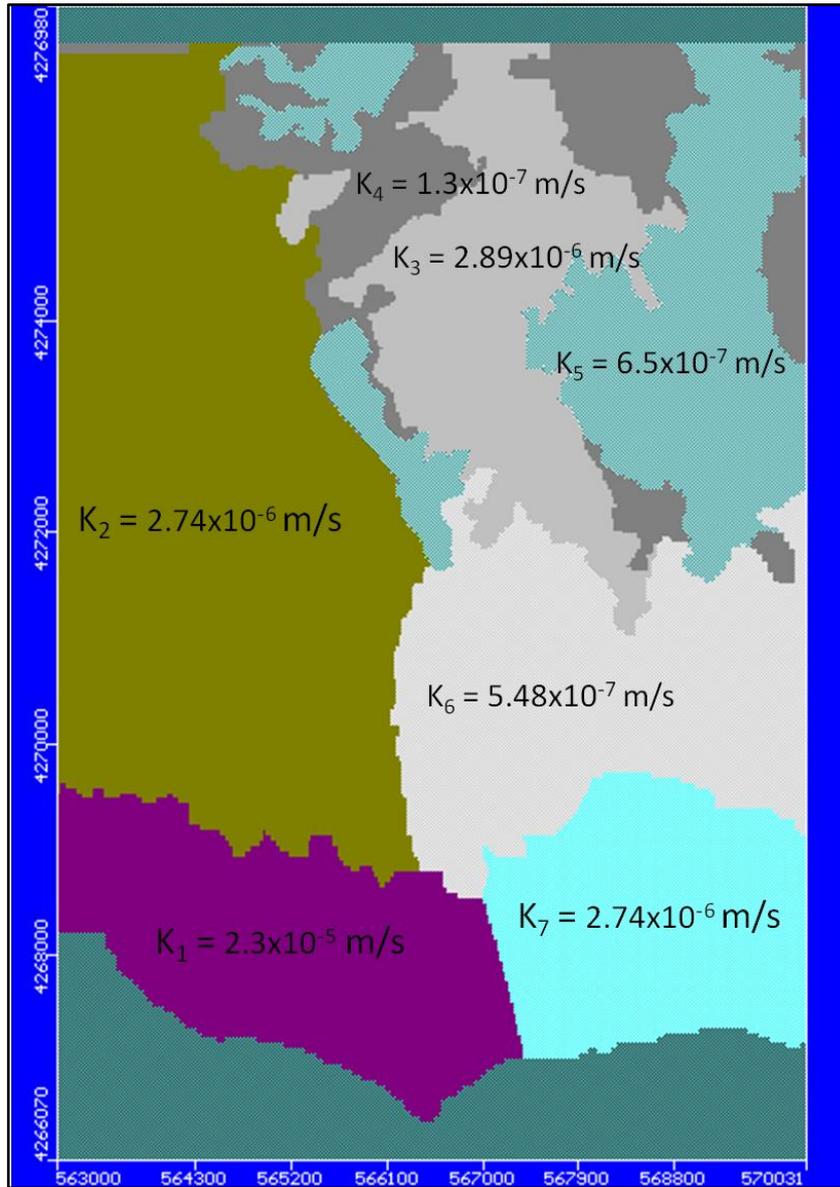
Figure 37 Hydraulic conductivity distribution in Layer 1 after calibration

In order to obtain a satisfying match between observed and calculated heads, boundary conditions were edited too. The general head boundary at the northern border was edited via changing boundary head and boundary distance values. Additionally, conductance values of the drains denoting the

71

seasonal creeks were modified. In the conceptual model, the drain conductance value was assigned as 1000 m²/day uniformly; however during calibration this value was increased to 3000 m²/day in some regions. In regions where the calculated heads were significantly higher than the observed ones and when change of hydraulic conductivity was not enough for obtaining a good match, drain conductance was increased. With trial and error, 3000 m²/day was found to be the most satisfying value.

4.4.2 Calculated Groundwater Budget

Using the calculated groundwater budget, it is possible to examine the recharge and discharge mechanisms of the model domain. Depending on the results of the steady-state model, components of the groundwater budget calculated under equilibrium conditions were examined. The groundwater budget calculated at the end of calibration for the whole domain is given in Table 9. The model domain is recharged from precipitation (4.63 hm³/yr), from flow along northern and northwestern boundaries (24.13 hm³/yr) and from Gediz River (2.50 hm³/yr), which make a total recharge of 31.26 hm³/yr. In the system, as expected there is balance between recharge and discharge. Furthermore; 49.2 % (15.37 hm³/yr) of the total recharge is discharged through wells, 32.5 % (10.17 hm³/yr) as subsurface outflow, 15.4 % (4.82 hm³/yr) from creeks, 1.6 % (0.50 hm³/yr) via evapotranspiration and 1.3 % (0.40 hm³/yr) through Gediz River.

Table 9 Calculated groundwater budget for the whole domain

Recharge (hm³/year)		Discharge (hm³/year)	
Precipitation	4.63	Wells	15.37
Subsurface Inflow	24.13	Subsurface Outflow	10.17
Gediz River	2.50	Gediz River	0.40
		Creeks	4.82
		Evapotranspiration	0.50
Total Recharge	31.26	Total Discharge	31.26

4.4.3 Sensitivity Analysis

Results of sensitivity analysis play an important role in minimization of model errors. The analysis is carried out by changing one parameter at a time while keeping others constant. In this study, a series of simulations were performed in order to test the sensitivity of the calibrated model to hydraulic conductivity, recharge and drain conductance changes. Hydraulic conductivity values of the laterites, ultramafic units and the limestones were changed independently, and resulting RMS and Normalized RMS values were plotted. Hydraulic conductivity coefficients for each unit were 0.25, 0.5, 1.5, 2, 2.5 and 3. The coefficient "1" corresponds to the hydraulic conductivity value of the calibrated model. It is important to note that; while multiplying the hydraulic conductivity of the selected unit in the first layer, hydraulic conductivity values of the lower layers were also multiplied with the same coefficient; i.e. the ratio between layers was kept constant. Resulting sensitivity analysis plots are presented in Figure 38, 39 and 40. According to these plots, the model is most sensitive to decrease in hydraulic conductivity of laterite. RMS values significantly increase when hydraulic conductivity of

laterite is lowered; however slight changes in RMS error are observed when conductivity is increased. For ultramafic units and limestones, sensitivity analysis shows that the model is more sensitive to decrease in hydraulic conductivity rather than the increase. When the figures are examined; it is seen that even when the coefficient is different than 1, RMS values slightly smaller than the calibrated model's, are observed. This is because of the fact that even though a smaller RMS is produced, the match between observed and calculated heads is not as successful as it is in the model accepted as calibrated and denoted with coefficient "1" in the sensitivity analyses.
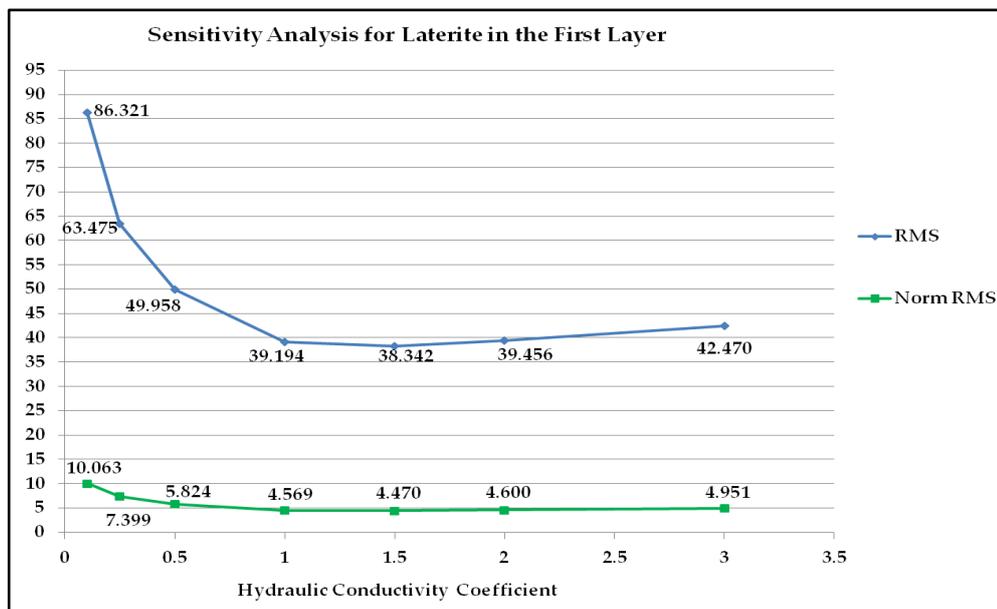

Figure 38 Sensitivity analysis for Laterite in the First Layer
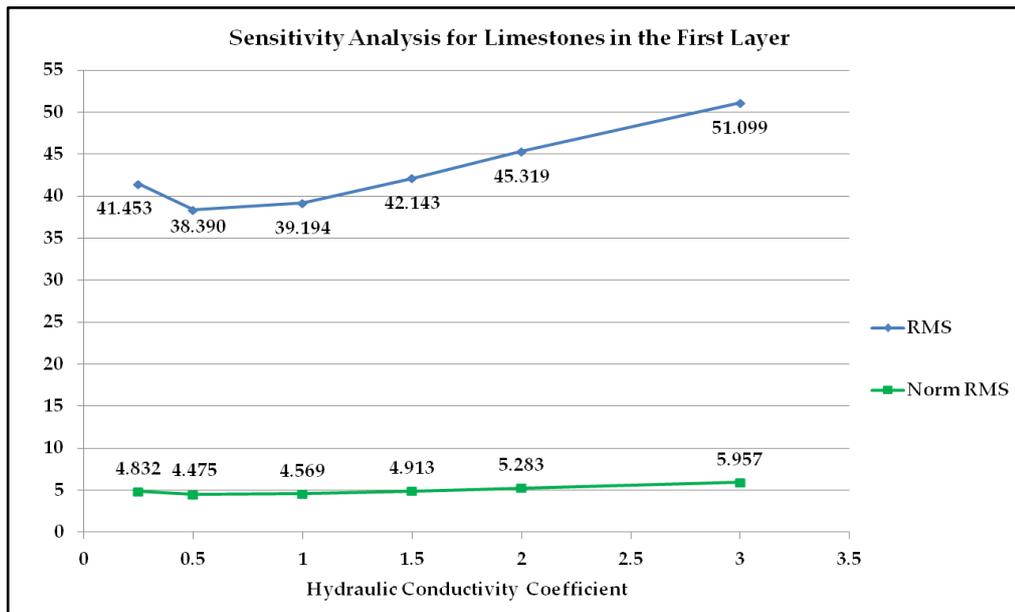
Figure 39 Sensitivity analysis for ultramafics in the first layer
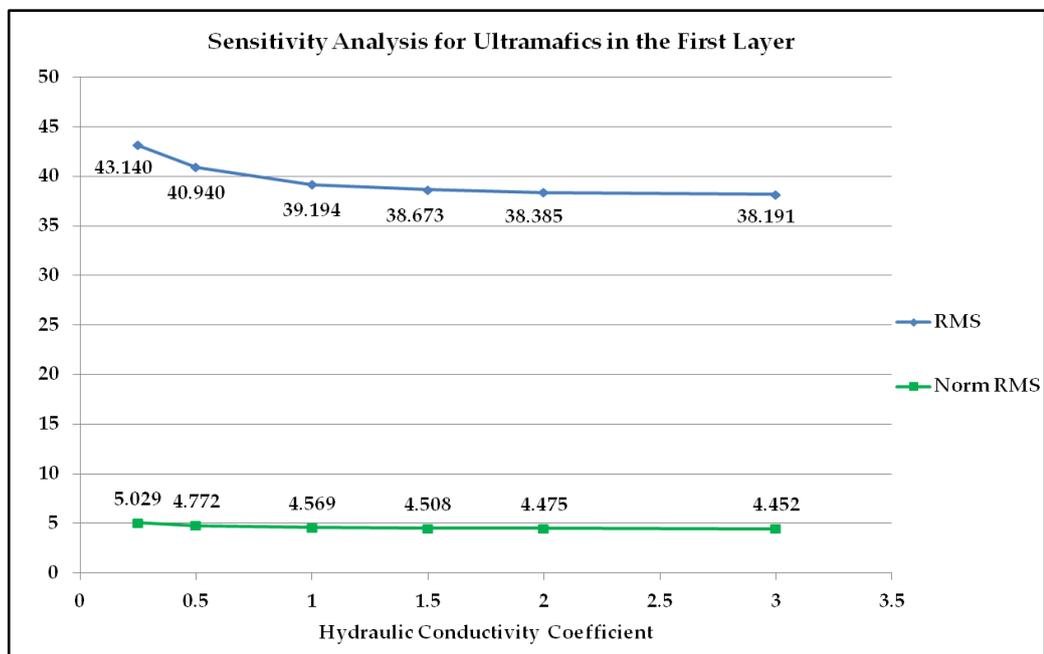
Figure 40 Sensitivity analysis for limestones in the first layer

Recharge coefficients in the sensitivity analysis were 0.25, 0.5 and 1.5. As can be depicted from Figure 41, the model is more sensitive to decrease in recharge rather than increase in it. Furthermore, when recharge is 1.5 times the value in the calibrated model, smaller RMS and Normalized RMS values are obtained, however the water levels in this simulation do not match with the observed heads as much as the calibrated model.
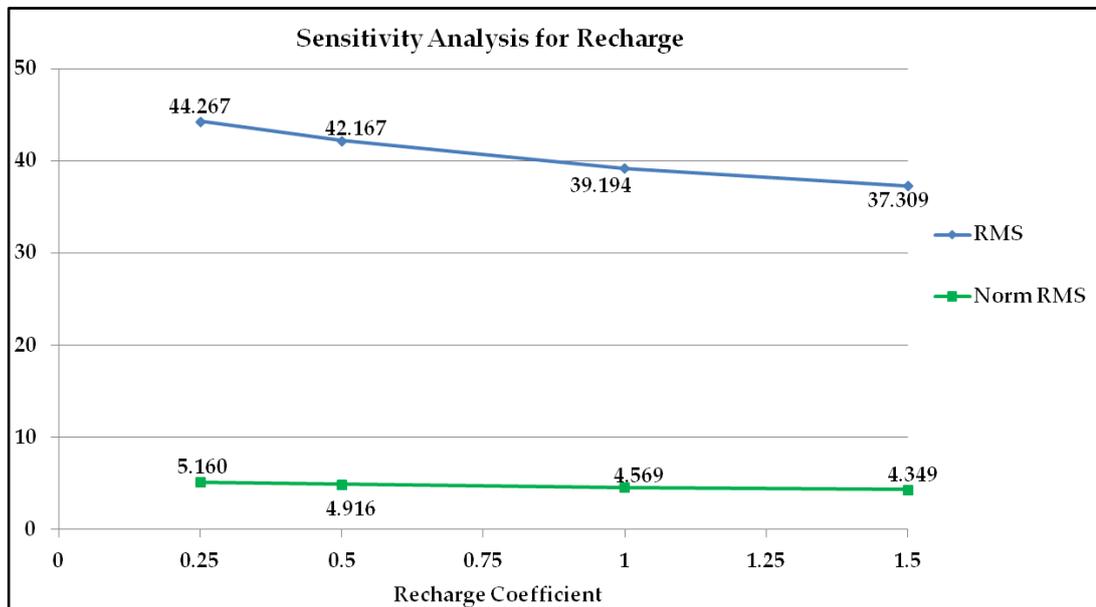
Figure 41 Sensitivity analysis for recharge

Finally, a sensitivity analysis was carried out for drain conductance, with coefficients 0.1, 0.5 and 1.5. In Figure 42, it can be seen that changes in drain conductance cause slight changes in RMS and Normalized RMS values; thus the system is not sensitive to changes in drain conductance.
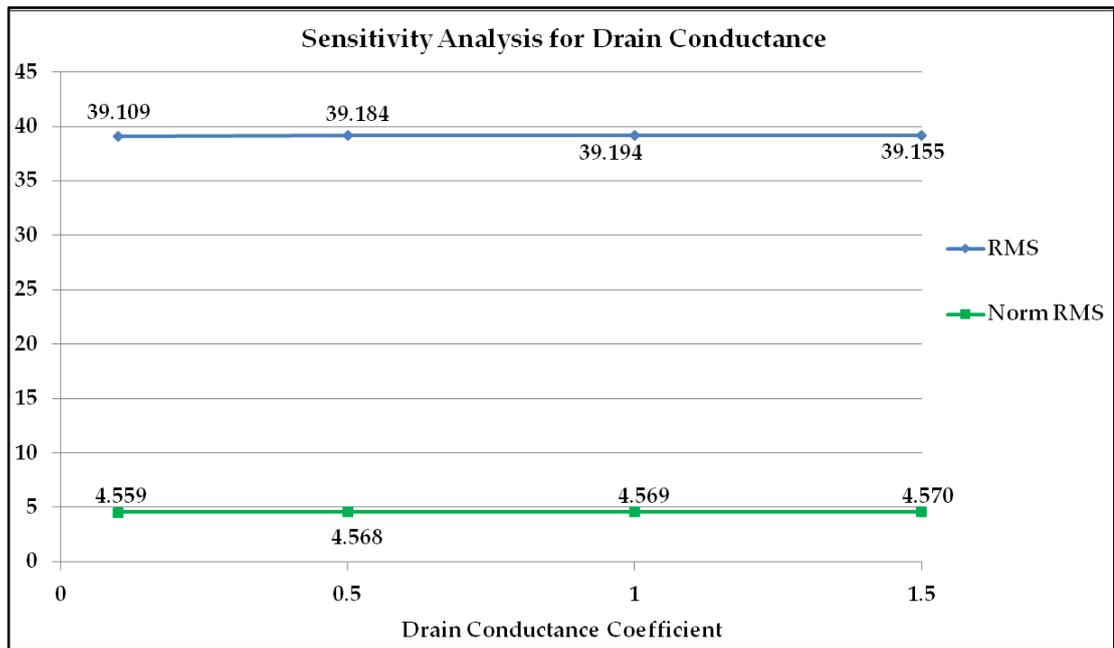
Figure 42 Sensitivity analysis for drain conductance

CHAPTER 5

DEWATERING SIMULATIONS

5.1 Methodology

The calibrated steady-state model has been applied to predict mine dewatering requirement for the proposed 15-year mine life. In the transient model, open-pit mining is represented by drain cells. In the active mining areas, the drain cells were specified with drain elevations set equal to bench elevations.

The drain cell configuration was determined by pit boundaries that are shown in Figure 43. The progressive advancement of pits due to mine schedule is represented in monthly time steps. The areas where excavation has not yet started, drain elevation is set equal to 1000 m, which is high above the water levels and is considered inactive by the software. Each active drain cell invert elevation corresponds to different time intervals during which excavation will reach to the pit bench elevations at the drain node. As the excavation progresses and parts of the pits are backfilled, the corresponding drain cells are de-activated. The aim of in-pit drain cells is to use total outflow from drains to predict groundwater inflow rate to the mine, which will yield the dewatering requirement.
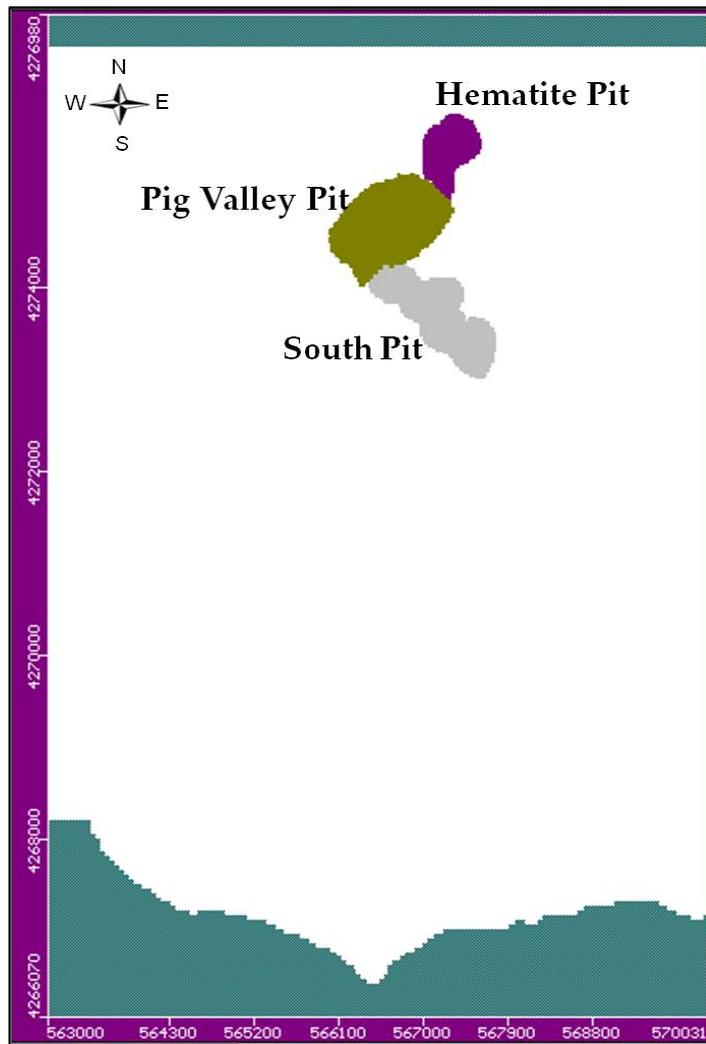
Figure 43 Pits represented by drains in the model

The drain cell conductance parameter represents the resistance to flow from saturated rocks into the drain cells, so is a critical parameter in determining inflow into pits. In the model, 10 m²/day conductance value was selected after trial of 1 m²/day, 5 m²/day and 1000 m²/day values. The results showed that 1 m²/day and 5 m²/day drain conductance values were not enough to obtain the required drawdowns and 1000 m²/day conductance value resulted in drawdowns more than the required ones.

The 15-year mine life was divided into 178 time steps, each time step corresponding to 1 month (30 days). In the first two months of 15 years, the excavation does not start, allowing preparation of the mining infrastructure including construction of roads, drainage and waste dump (Dagdelen and Gungor, 2010).

5.2 Predicted Flow Rates

The open pits are located in laterite, which bears the nickel to be mined. Hydraulic conductivity of laterites is one of the main parameters controlling the groundwater inflow rate into open pits. In order to determine the hydraulic conductivity of the laterites four wells were drilled into laterites and tested. However, three of these wells were dry, leaving only one pump tested value for hydraulic conductivity of laterites. Furthermore, this value is expected to be an elevated value since the pump tested well is located on a fault extending through Pig Valley and passing through this monitoring location. Although model calibration was conducted using this value for hydraulic conductivity of laterites, there is a significant uncertainty associated with it. Hence, due to this uncertainty in hydraulic conductivity of laterite, a sensitivity analysis was carried out in order to assess its affect on the calculated inflow rates into pits. While all other parameters were kept constant, hydraulic conductivity of laterite was multiplied by coefficients 0.1, 0.25, 0.5 and 1.5; the results are shown in Table 10. As seen in the table; when the hydraulic conductivity of laterite in the calibrated model is used, this flow rate is 107.58 L/s. When the hydraulic conductivity of laterite is reduced tenfold, the flow rate decreases three fourths, to 24.42 L/s.

Table 10 Change of flow rates with the change of hydraulic conductivity of laterite

	Hydr. Cond. Coefficients of Laterite	Lat_1.5	Lat_1	Lat_0.5	Lat_0.25	Lat_0.1
Hematite Pit	Flow Rate (L/s)	51.47	59.41	54.37	44.38	31.49
	Duration of Dewatering	13 months	13 months	17 months	17 months	16 months
Pig Valley Pit	Flow Rate (L/s)	142.16	98.94	64.03	38.55	25.55
	Duration of Dewatering	143 months	140 months	102 months	102 months	102 months
South Pit	Flow Rate (L/s)	77.40	40.81	24.75	5.07	1.57
	Duration of Dewatering	45 months	45 months	15 months	15 months	10 months
Pits Average *	Flow Rate (L/s)	156.93	107.58	58.41	35.54	24.42
	Duration of Dewatering	156 months	153 months	134 months	134 months	128 months

* Due to different durations of dewatering in each pit, weighted average is used in this calculation.

The flow rates in the pits were summarized in Table 10; however as mentioned, duration of dewatering changes in each pit. Also, the flow rates display high variations with time in each pit. In Figure 44, time versus flow rate plots of each pit separately and the total for all pits are given. These results are obtained from the simulation carried out using hydraulic conductivity of laterite in the calibrated model (K_{lat} = 2.89x10^{-6} m/s). In the

figure, when flow rates are equal to zero there is no inflow to the pits; in this case either no dewatering is required or the dewatering applied for another pit produces the required drawdown in this pit too. Inferred from the figure is that, the maximum flow rate at Hematite Pit is 111.5 L/s; at Pig Valley Pit, 319.4 L/s and at South Pit, 141.3 L/s. In this case, the total maximum flow rate is encountered in Pig Valley pit, being equal to 319.4 L/s. This observation is very consistent since the maximum required drawdown is also expected from Pig Valley Pit as mentioned before. Furthermore; as given in Table 10, the calculated average flow rate considering all the pits and their different durations of dewatering is 107.58 L/s.

As it can be implied from Figure 44, the general trends in flow rates are in accordance with the timewise development of pits. Increasing trends in flow rates correspond to the progress of excavation. On the contrary, the decreasing trends correspond to the decrease in dewatering requirement. Despite the general increasing trends, small fluctuations in flow rates are observed. The ascendant parts correspond to excavation of new pit benches, and after the targeted bench elevation is reached, the bottom elevation of pit stabilizes until the next bench excavation. Meanwhile, the dewatering rate starts decreasing causing a descendent portion in the plot. With the continuation of excavation of new benches, a cyclic fluctuation in the plot occurs. When the maximum flow rate is observed at day 3000, last two stages of Pig Valley Pit and three stages of South Pit are active; which is consistent with the high requirement of dewatering. As previously mentioned; the times when flow rates are zero denote that either no dewatering is required or the dewatering applied for another pit produces the required drawdown in this pit too.
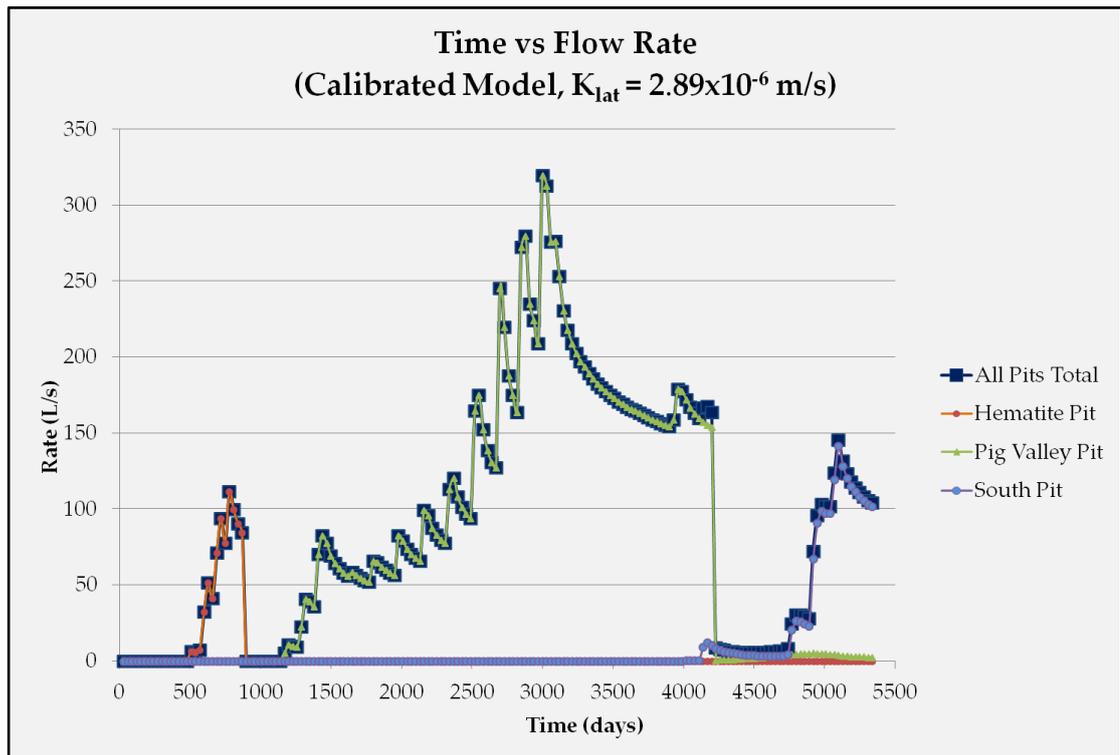
Figure 44 Time versus flow rate plot for each pit separately and the total for all pits (for the calibrated model)

Figure 45 was plotted from the results obtained from the simulation carried out using hydraulic conductivity of laterite in the calibrated model multiplied by 0.1 ($K_{lat} = 2.89 \times 10^{-7}$ m/s). In this case, the maximum flow rate at Hematite Pit is 60.6 L/s; at Pig Valley Pit, 91.9 L/s and at South Pit, 2.7 L/s. The total maximum flow rate, being equal to 91.9 L/s, is again observed in Pig Valley pit and this is consistent with the expectation of maximum required drawdown in Pig Valley Pit. In this figure, the trends and cyclic fluctuations are similarly observed as in Figure 41, the only difference is the minor dewatering requirement of South Pit due to low initial water levels. The dewatering applied to other pits is very effective for the water levels to

be lowered in South Pit; consequently, dewatering in this pit is required for a limited time, with a very small flow rate (1.57 L/s).
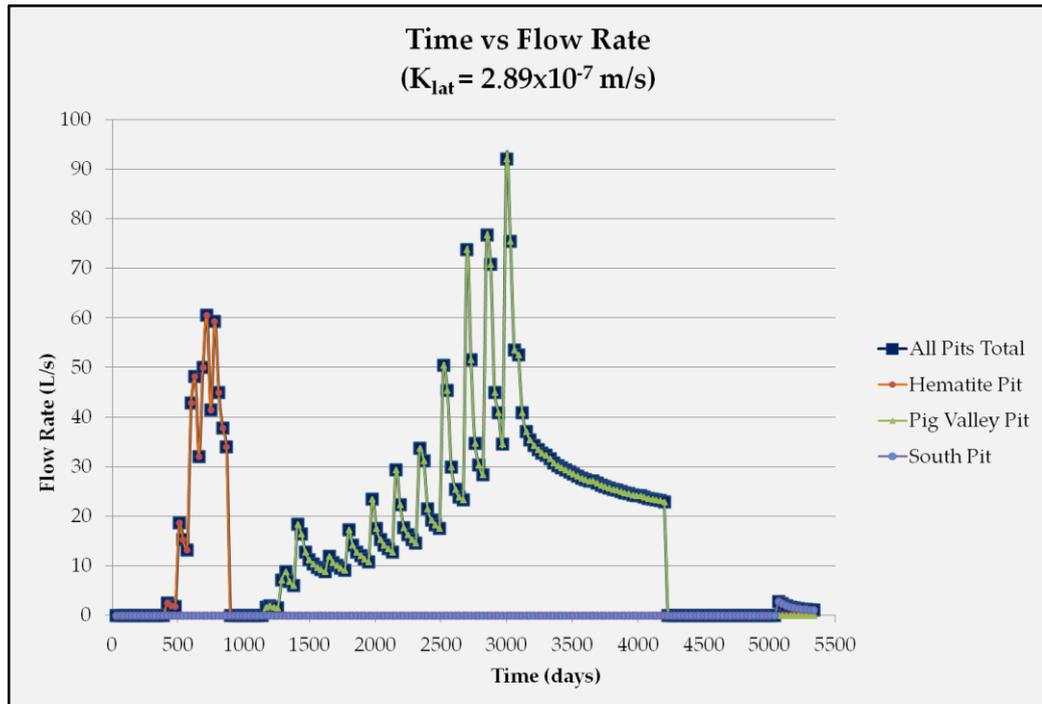

Figure 45 Time versus flow rate plot for each pit separately and the total for all pits (for one tenth of hydraulic conductivity of calibrated model)

5.3 Water Levels in the Pits

In order to check whether the water levels in the pits are lowered to the required elevations, four representative observation locations D-1, D-2, D-3 and D-4 were selected (Figure 46). Water levels in these locations are displayed in Figure 47, 48, 49 and 50 together with initial heads and

corresponding pit bench elevations as mining progresses. The displayed results belong to the simulation carried out using hydraulic conductivity of laterite in the calibrated model (i.e. it equals to 2.89×10^{-6} m/s). In Figure 47, it is observed that in central part of Hematite Pit the initial water level is high above the lowest bench elevation. When the timewise change of water level and mining is examined, it is seen that the target drawdown is produced and the water level is lowered below the pit bottom for dry mining conditions. The first time when water level starts bouncing back corresponds to the end of excavation in Hematite Pit (the time when drains were deactivated), the following up and downs are effects of ongoing dewatering in other pits.
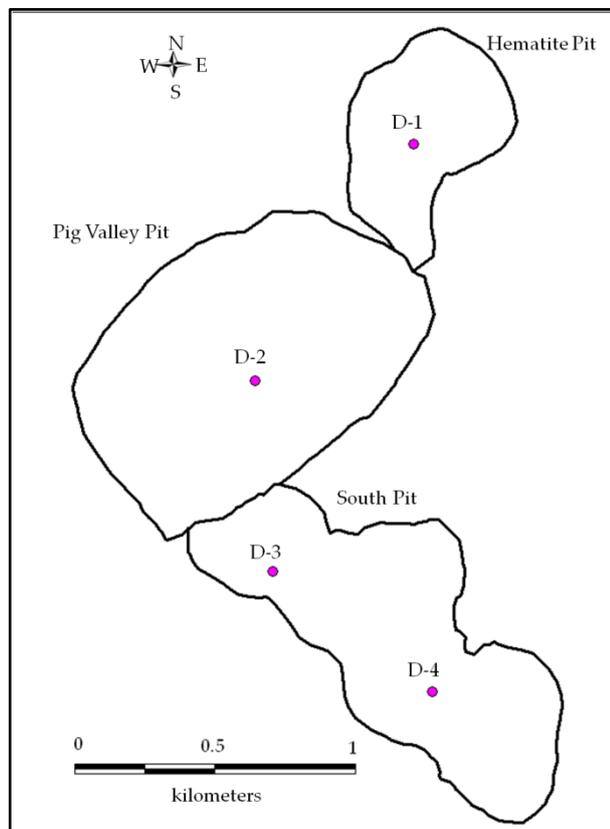

Figure 46 Observation locations
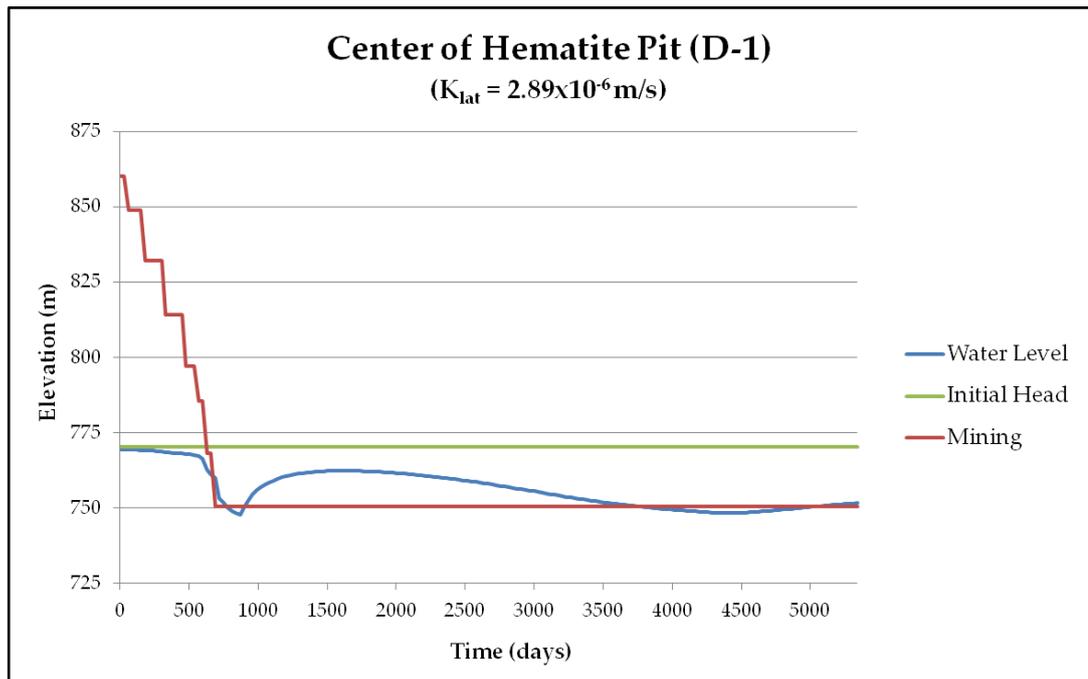
**Figure 47** Initial head, water level and mining progress in the center of

Hematite Pit

In Figure 48, it is seen that groundwater inflow is a problem for Pig Valley Pit for most of its excavation. It is clear that, water level is successfully lowered below the pit bench elevations when required. The time when water level starts to recover (day 4200) corresponds to the cessation of mining in Pig Valley Pit.
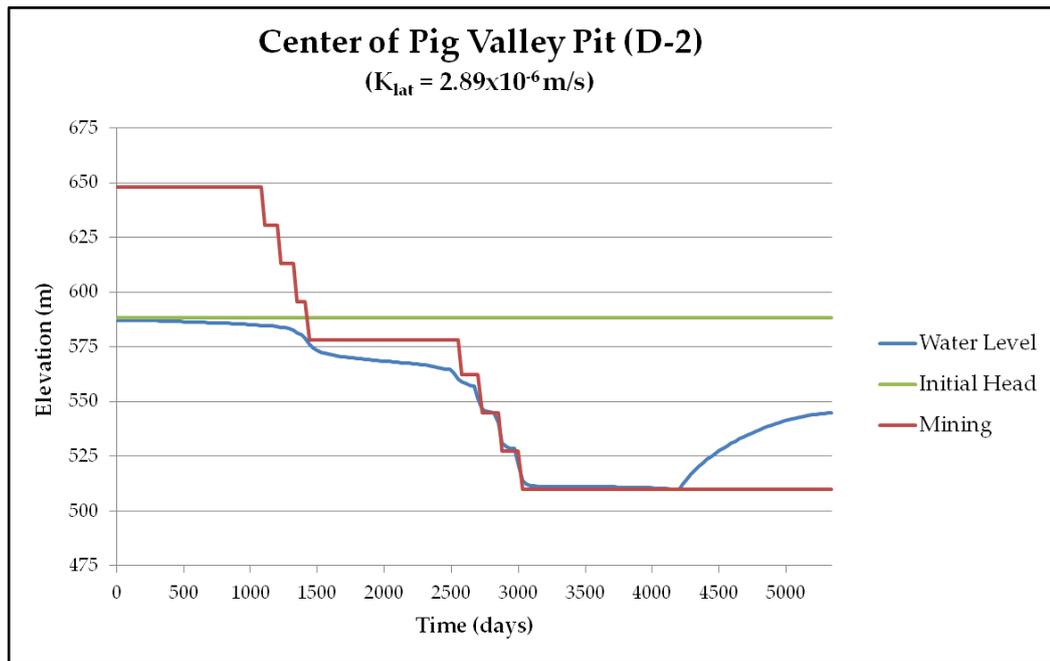
Figure 48 Initial head, water level and mining progress in the center of Pig Valley Pit

Figure 49 displays the timely change of water level and pit bench elevations in northern part of South Pit. From the figure it can be concluded that this part of the pit requires dewatering in the last two years of excavation, it should be noted that South Pit is the last pit to be mined in the area. The required drawdowns in the pit are obtained for most of the excavation time, however at the last time steps, since dewatering in other pits lasted and mining in the whole area is about to finish, the required water levels cannot be reached. As mentioned before, South Pit is excavated in four stages. Mining in this pit starts in the southern parts, and then continues in northern areas during the last stages. For this reason, the decline in water levels before

the initiation of excavation is the result of ongoing dewatering in the southern parts of this pit together with Pig Valley Pit.
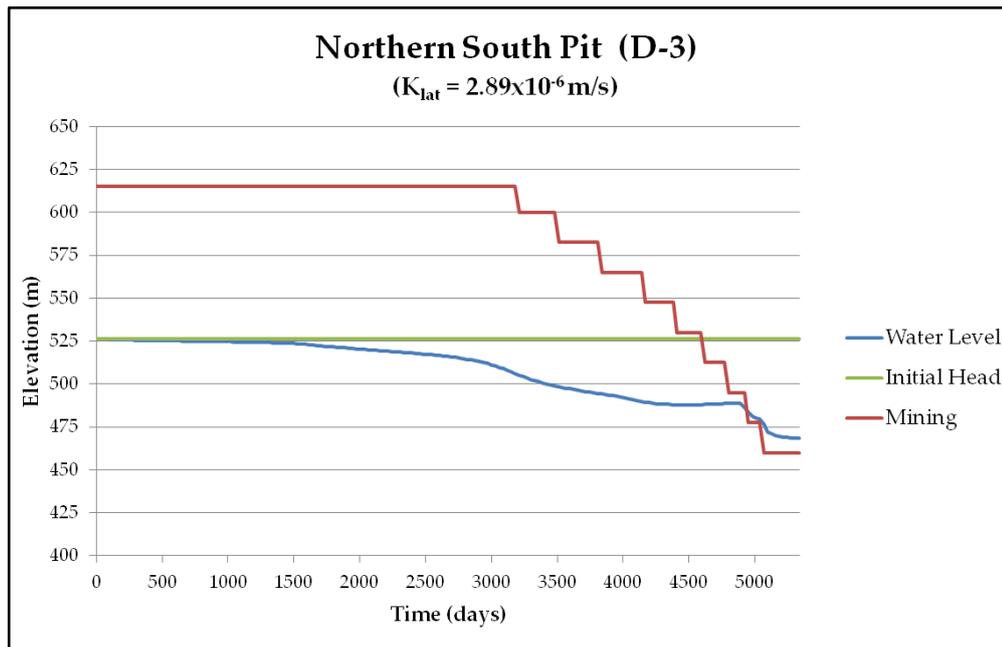

Figure 49 Initial head, water level and mining progress in northern part of South Pit

Figure 50 displays that in the central parts of South Pit, the dewatering requirement is not excess and the required drawdown is successively produced.
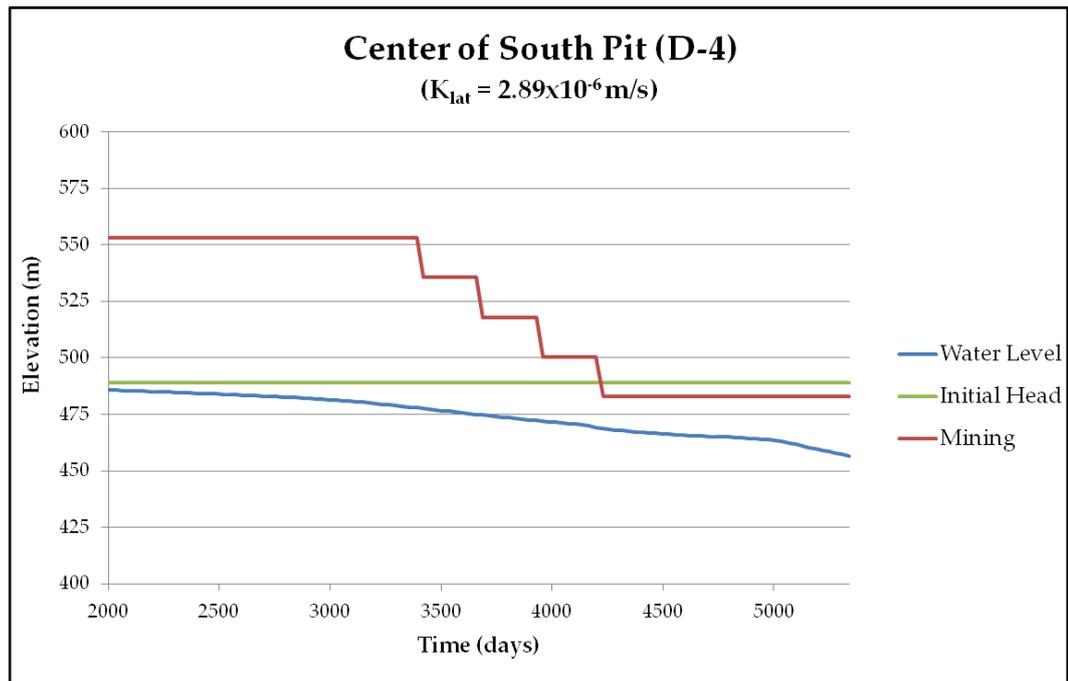
Figure 50 Initial head, water level and mining progress in center of South Pit

In order to assess the effects of change in hydraulic conductivity, results of the simulation in which hydraulic conductivity of laterite is multiplied by 0.1 (i.e. it equals to 2.89×10^{-7} m/s) are also presented for the same observation points (D-1, D-2, D-3 and D-4) in Figures 51, 52, 53 and 54, respectively. When the hydraulic conductivity of the laterite is reduced by tenfold the simulated steady-state water levels in the Pig Valley Pit and South Pit were lowered significantly while they were slightly elevated in the Hematite Pit. Since the heads obtained from steady-state model run were used as initial conditions for the transient dewatering simulations, there were significant differences in the dewatering requirements resulting from different initial conditions. Coupled with low hydraulic conductivity of the laterite, the low initial head produced less dewatering flow rates.

The results show that in Hematite Pit and Pig Valley Pit, the required drawdown is achieved successfully as can be seen in Figures 51 and 52, respectively. In both figures, the times when water levels start bouncing back correspond to the cessation of excavation in these pits. In the South Pit, both in the northern and central parts the initial water levels are below the pit bench elevations during all the excavation time (Figures 53 and 54). At the selected locations, dewatering requirement is not necessary but for other regions of the South Pit there is the requirement of dewatering, however it is far too less compared to the other pits.
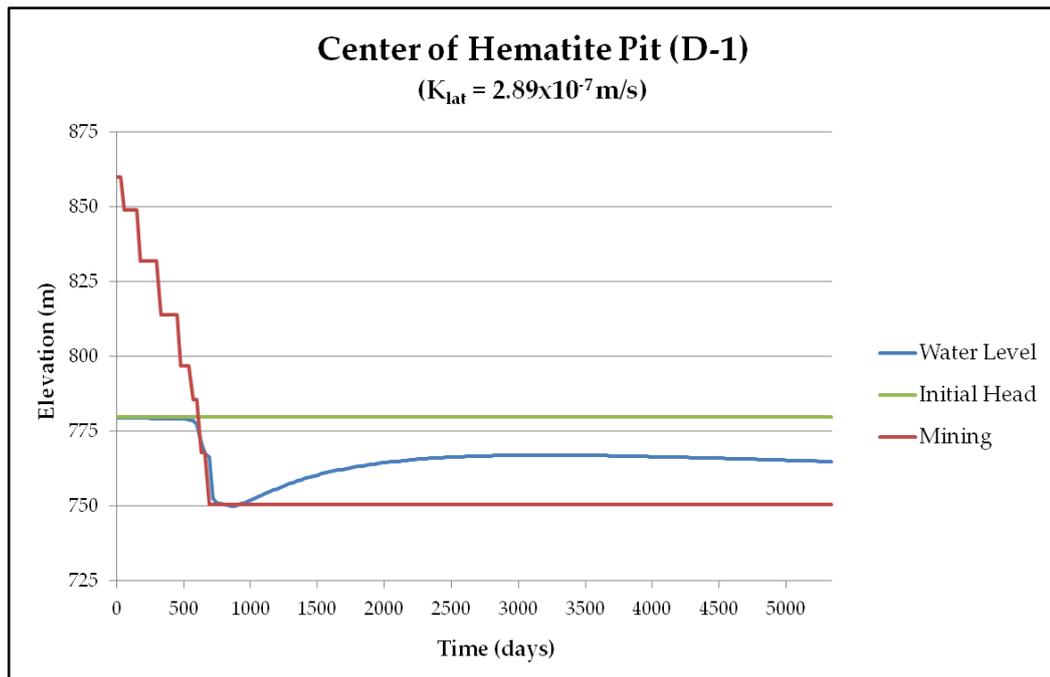

Figure 51 Initial head, water level and mining progress in the center of Hematite Pit
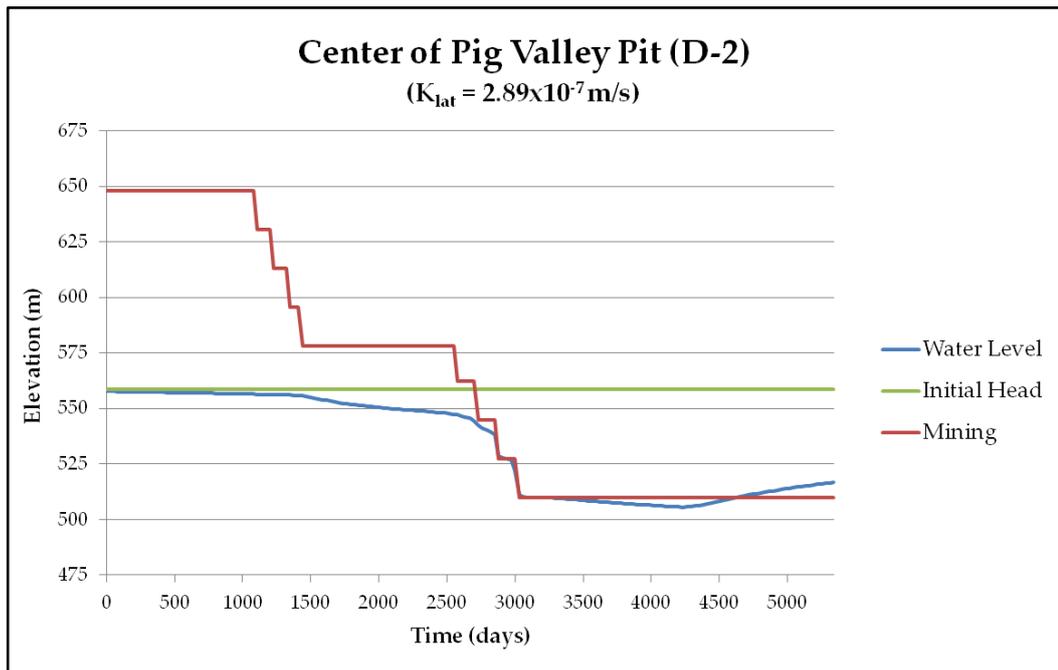
Figure 52 Initial head, water level and mining progress in the center of Pig
Valley Pit
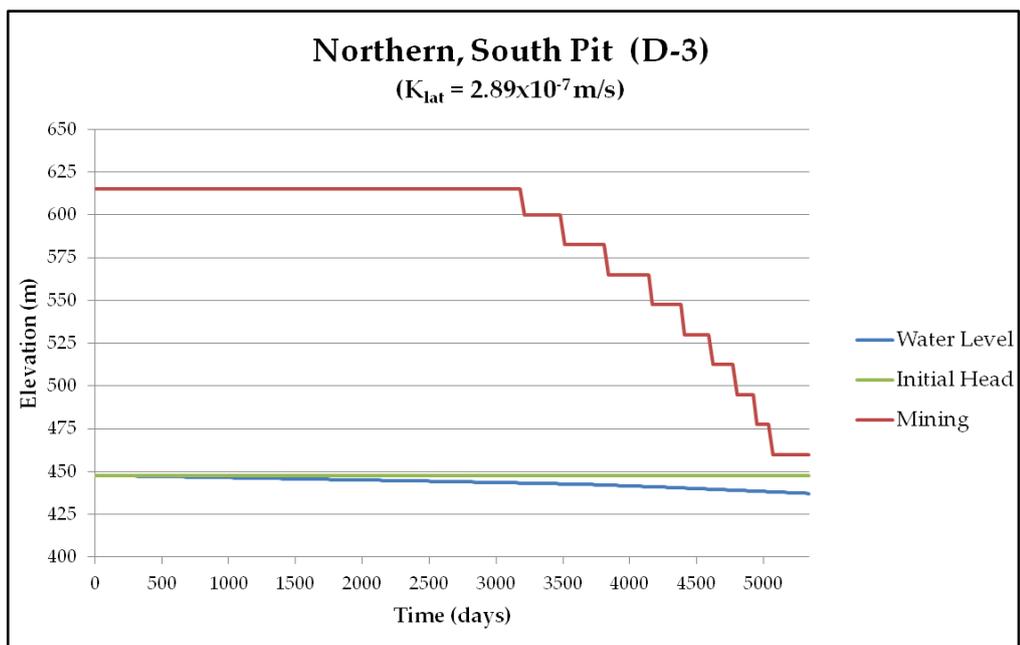
Figure 53 Initial head, water level and mining progress in northern South Pit

91
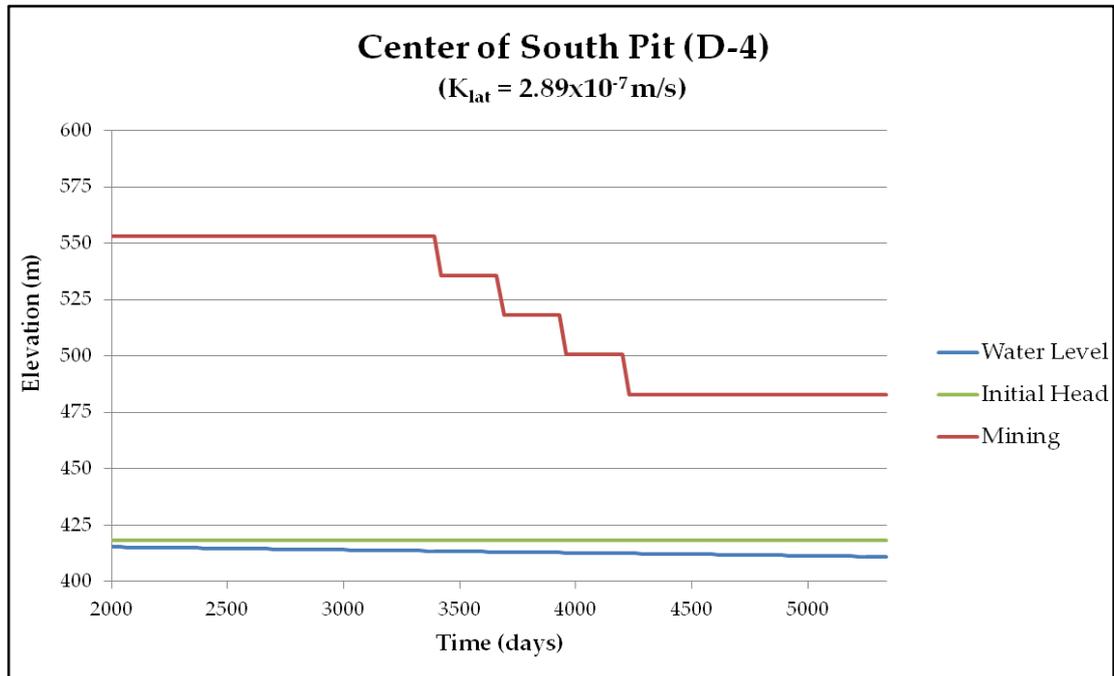
Figure 54 Initial head, water level and mining progress in center of South Pit

CHAPTER 6

CONCLUSION AND RECOMMENDATIONS

The purpose of this study was to assess the dewatering requirements of planned open pit nickel mining at Çaldağ Site in Western Turkey. With excavation of three open pits, 15 years of mining is proposed in Çaldağ. With the progress of mining, penetration of water table will be encountered and this will cause groundwater inflow to the mine. For safe and efficient conditions together with pit wall stability in the mine, dewatering is crucial. This study was carried out to predict the rate at which the dewatering should be accomplished.

In order to characterize the study area; a conceptual model was developed using geology, hydrogeology, meteorology and hydrology data. Consequently, a numerical groundwater model based on this conceptual model was set up, using MODFLOW. After calibration of this model with existing field data, dewatering simulations were carried out to predict the dewatering rate. In the dewatering simulations, a transient model covering the proposed 15-year mine life with monthly time steps was utilized. In this model, open-pit mining was represented by drain cells, using MODFLOW Drain Package. In the active mining areas, the drain cells were specified with drain elevations set equal to bench elevations. The configuration of drain cells was determined by pit boundaries, and the progressive advancement of pits based on the mine schedule was represented in monthly time steps. The

purpose of using in-pit drain cells was to use the outflow from drains to calculate the inflow rate to the mine. In order to obtain dry conditions in the pits, the dewatering rate should be at least equal to the inflow rate into the mine.

Based on the data from calibrated steady-state model; when all pits are taken into account, the average flow rate was determined to be 107.58 L/s. Because the hydraulic conductivity of laterite is one of the main parameters controlling the flow rate into the pits and due to lack of sufficient data regarding this parameter, it was essential to assess the impact of this parameter on the pit inflow rates. Therefore, simulations were carried out for a range of different laterite hydraulic conductivities (hydraulic conductivity coefficients of 0.1, 0.25, 0.5 and 1.5 were used). In the calibrated model; 2.89×10^{-6} m/s, determined by pumping test, was used. A tenfold reduction in the hydraulic conductivity of laterite (2.89×10^{-7} m/s) resulted in three fourths of decrease in the flow rate (24.42 L/s).

Since nickel is extracted from the laterite, hydraulic conductivity of laterites is one of the main parameters controlling the groundwater inflow rate into open pits. Due to lack of sufficient data regarding hydraulic conductivity of laterites, a sensitivity analysis was carried out and a range of flow rates were calculated for different hydraulic conductivity values. Hence, in order to confirm the hydraulic conductivity of laterites and obtain a realistic flow rate for dewatering, further tests aiming the hydraulic conductivity distribution in laterites are needed.

For the results of this study to be put into practice, with new simulations a dewatering plan should be developed in future studies. During operation of the mine while dewatering is active, the model should be continuously updated with discharge and water level data from the dewatering system. In addition, further modeling studies evaluating the recovery of water levels within the pits following the cessation of mining are recommended.

REFERENCES

Ağartan, E., 2010, Assessment of Water Supply Impacts for A Mine Site in Western Turkey. Master's thesis, Middle East Technical University.

Bozkurt, E., and Rojay, B., 2005, Episodic , Two-stage Neogene Extension and Short-Term Intervening Compression in Western Turkey: Field Evidence from the Kiraz Basin and Bozdag Horst. Geodinamica Acta, 4, 299-316.

Bozkurt, E., and Satir, M., 2000, The Southern Menderes Massif (Western Turkey): Geochronology and Exhumation History. Geological Journal, 35(3-4), 285-296.

Bozkurt, E., and Sözbilir, H., 2004, Tectonic Evolution of the Gediz Graben: Field Evidence for an Episodic, Two-stage Extension in Western Turkey. Geological Magazine, 141(1), 63-79.

Bruce, I. G., 2006, Open Pit Dewatering Numerical Modelling Report, BGC Engineering, 41 p.

Büyükakıncı, E., and Topkaya, Y. A., 2009, Extraction of Nickel from Lateritic ores at Atmospheric Pressure with Agitation Leaching. Hydrometallurgy, 97(1-2), 33-38. Elsevier B.V.

Çiftçi, N. B., and Bozkurt, E., 2009, Evolution of the Miocene sedimentary Fill of the Gediz Graben, SW Turkey. Sedimentary Geology, 216(3-4), 49-79. Elsevier B.V.

Dağdelen, K., and Güngör, A., 2010, Mine Planning and Production Schedule of Caldag Nickel Project, 35 p.

Duru, U., 2004, Dewatering Plan and Prediction For Pit Lake Flooding for a Quarry Site. Master's thesis, Middle East Technical University.

Farrington, V., and MacHunter, C., 2007, Hydrogeological Assessment of the Maud Creek Gold Project. Terra, 39 p.

Göveli, A., 2006, Nickel Extraction From Gordes Laterites by Hydrochloric Acid Leaching, Master's thesis, Middle East Technical University.

Harbaugh, A. W., Banta, E. R., Hill, M. C., and McDonald, M. G., 2000, MODFLOW-2000, The U.S. Geological Survey Modular Ground-Water Model: User Guide to Modularization Concepts and the Ground-Water Flow Process, U.S. Geological Survey, Open-File Report 00-92.

Kuchling, K., Chorley, D., and Zawadzki, W., 2000, Hydrogeological Modeling of Mining Operations at the Diavik Diamonds Project.

Morton, K. L., and Van Mekerk, F. A., 1993, A Phased Approach to Mine Dewatering. Mine Water and the Environment, 12(Annual), 27-34.

Oxley, A., Sirvanci, N., and Purkiss, S., 2007, Çaldağ Nickel Laterite Atmospheric Heap Leach Project. Metalurgija –Journal of Metallurgy (MJoM), 13(1), 5-10.

Philippson, A., 1915, Reisin Und Forsehungen in Westliehen Klainasien: Pet. Mitt. Erg. M. 167, 173, 177, 1980, Cotha.

Schlumberger Water Services, Visual MODFLOW – Dynamic Groundwater Flow and Contaminant Transport Modeling Software, 2010, Canada.

Shepherd, R., 1993, Ancient Mining. Elsevier, 494 p; Elsevier B.V.

Singh, R. N., and Reed, S. M., 1988, Mathematical Modelling for Estimation of Minewater Inflow to a Surface Mining Operation. International Journal of Mine Water, 7(3), 1-33.

Soil Conservation Service, 1964, SCS National Engineering Handbook, Section 4: Hydrology, Updated 1972, U.S. Department of Agriculture, Washington D.C.

Thorne, R., Herrington, R., and Roberts, S., 2009, Composition and origin of the Çaldağ oxide nickel laterite, W. Turkey. Mineralium Deposita, 44(5), 581-595.

University of Stuttgart, Institute of Applied and Experimental Mechanics, Boundary Element Methods, http://www.iam.uni-stuttgart.de/bem/home_bem_introduc.html (accessed September 2, 2011).

Williamson, S., and Vogwill, R. I. J., 2001, Dewatering In the Hot Groundwater Conditions at Lihir Gold.

Wolkersdorfer, C., 2008, Water Management at Abandoned Flooded Underground Mines. Quality Assurance, 465 p, Springer.

Yanik, G., Uz, B., and Esenli, F., 2006, Turgutlu (Manisa) yöresi Neojen çökellerinin jeolojisi. İTÜ Dergisi, 5(2), 49-58.

Yazıcıgil, H., 2008, Hydrogeological Characterization of Çaldağ Nickel Mine Project Area, Sardes Nikel Madencilik A.Ş. Quality, 128 p.

Yilmaz, Y., Genc, S. C., Gürer, F., Bozcu, M., Yılmaz, K., Karacık, Z., and Altunkaynak, S., 2000, When Did the Western Anatolian Grabens Begin to Develop?, Geological Society, London, Special Publications, 173(1), 353-384.